

# Design and Synthesis of Amphiphilic Xanthone-Based, Membrane-Targeting Antimicrobials with Improved Membrane Selectivity

Hanxun Zou,<sup>†,‡,◆</sup> Jun-Jie Koh,<sup>†,§,◆</sup> Jianguo Li,<sup>†,||</sup> Shengxiang Qiu,<sup>⊥</sup> Thet Tun Aung,<sup>†</sup> Huifen Lin,<sup>†</sup> Rajamani Lakshminarayanan,<sup>†,○</sup> Xiaoping Dai,<sup>⊥</sup> Charles Tang,<sup>#</sup> Fang Hui Lim,<sup>†,▽</sup> Lei Zhou,<sup>†</sup> Ai Ling Tan,<sup>#</sup> Chandra Verma,<sup>†,||,▲</sup> Donald T. H. Tan,<sup>†,§</sup> Hardy Sze On Chan,<sup>▽</sup> Padmanabhan Saraswathi,<sup>†</sup> Derong Cao,<sup>\*,‡</sup> Shouping Liu,<sup>\*,†,○</sup> and Roger W. Beuerman<sup>\*,†,○</sup>

<sup>†</sup>Singapore Eye Research Institute, 11 Third Hospital Avenue, Singapore 168751, Singapore

<sup>‡</sup>School of Chemistry and Chemical Engineering, State Key Lab of Luminescent Materials and Devices, South China University of Technology, Guangzhou 510641, China

<sup>§</sup>Department of Ophthalmology, Yong Loo Lin School of Medicine, National University of Singapore, Singapore 119074, Singapore

<sup>||</sup>Bioinformatics Institute, Singapore 138671, Singapore

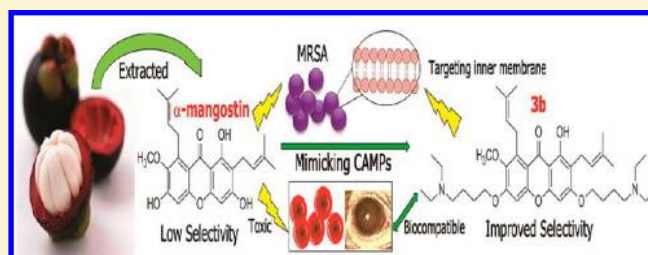
<sup>⊥</sup>Program for Natural Products Chemical Biology, Key Laboratory of Plant Resources Conservation and Sustainable Utilization, South China Botanical Garden, the Chinese Academy of Sciences, Guangzhou, China

<sup>#</sup>Department of Pathology, Singapore General Hospital, Singapore 169608, Singapore

<sup>▽</sup>Department of Chemistry, National University of Singapore, 3 Science Drive 3, Singapore 117543, Singapore

<sup>○</sup>Duke-NUS Medical School, SRP Neuroscience and Behavioral Disorders, Singapore 169857, Singapore

**ABSTRACT:** This work describes how to tune the amphiphilic conformation of  $\alpha$ -mangostin, a natural compound that contains a hydrophobic xanthone scaffold, to improve its antimicrobial activity and selectivity for Gram-positive bacteria. A series of xanthone derivatives was obtained by cationic modification of the free C3 and C6 hydroxyl groups of  $\alpha$ -mangostin with amine groups of different  $pK_a$  values. Modified structures using moieties with high  $pK_a$  values, such as AM-0016 (**3b**), exhibited potent antimicrobial properties against Gram-positive bacteria. Compound **3b** also killed bacteria rapidly without inducing drug resistance and was nontoxic when applied topically. Biophysical studies and molecular dynamics simulations revealed that **3b** targets the bacterial inner membrane, forming an amphiphilic conformation at the hydrophobic–water interface. In contrast, moieties with low  $pK_a$  values reduced the antimicrobial activity of the parent compound when conjugated to the xanthone scaffold. This strategy provides a new way to improve “hits” for the development of membrane-active antibiotics that target drug-resistant pathogens.



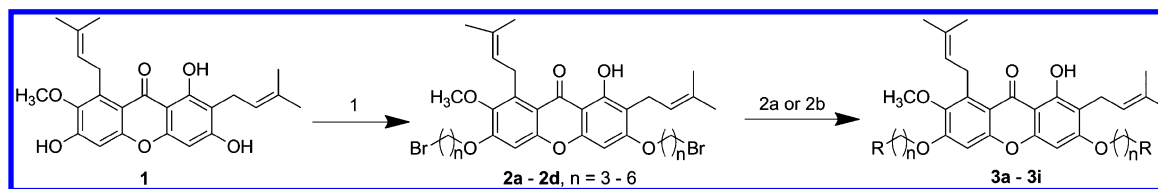
## INTRODUCTION

Antibiotic resistance is a critical global healthcare problem, which is widely associated with the failure of antibiotic treatment and previously treatable bacterial infections are now resulting in additional morbidity and healthcare costs.<sup>1–5</sup> The emergence of virulent and deadly multidrug resistance superbugs and pathogens such as methicillin-resistant *Staphylococcus aureus* (MRSA) exemplifies the continuing problem of resistance.<sup>3</sup> Studies have shown that Gram-positive bacteria such as MRSA are developing resistance to various antibiotics including  $\beta$ -lactams (oxacillin and ampicillin),<sup>6</sup> vancomycin,<sup>6</sup> fluoroquinolones,<sup>7</sup> linezolid,<sup>8</sup> and daptomycin.<sup>9</sup> Hence, there is a critical need for new therapeutic agents that are effective against multidrug-resistant pathogens.

We have recently reported that  $\alpha$ -mangostin, a natural xanthone extracted from a common Southeast Asian fruit, *Garcinia mangostana*, disrupts the cytoplasmic membrane of Gram-positive organisms including MRSA.<sup>10</sup> Membrane-

targeting antibiotics, in a similar fashion to natural antimicrobial peptides, are expected to pose less risk for the emergence of resistance.<sup>11</sup> In fact,  $\alpha$ -mangostin displays desirable antimicrobial properties such as a low minimum inhibitory concentration, rapid bactericidal action, and the avoidance of the development of resistance.<sup>10</sup> However,  $\alpha$ -mangostin does not show adequate selectivity between bacterial and mammalian cell membranes. The hydrophobic nature of the xanthone scaffold of  $\alpha$ -mangostin provides a strong driving force for lipid solvation into eukaryotic and prokaryotic membranes. To overcome these issues, new xanthone analogues with improved membrane selectivity are required. A thorough search of the literature shows that no clear design principles exist for modifying small molecules to make them more specific for bacterial membranes.<sup>11,12</sup>

**Received:** November 15, 2012

Scheme 1. Synthesis of Xanthone Analogues<sup>a</sup>

<sup>a</sup>Reagents and conditions: (1)  $\text{Br}(\text{CH}_2)_n\text{Br}$ ,  $\text{K}_2\text{CO}_3$ , acetone, reflux, 24 h; (2a) **3a–3g**, corresponding amine, dimethyl sulfoxide, RT, 4 h; (2b) **3h** and **3i**, corresponding azole or triazole,  $\text{K}_2\text{CO}_3$ , acetone, reflux, 48 h.

Generally, cationic antimicrobial peptides (CAMPs) contain hydrophobic and cationic residues and are able to adopt facial amphiphilic topologies.<sup>13–15</sup> Cationic groups are preferentially attracted to the anionic phospholipid head groups of the bacterial membrane due to electrostatic interactions.<sup>13,16</sup> In contrast, the CAMPs have relatively weaker interactions with neutral or zwitterionic amphiphiles that are present in mammalian membranes at physiological pH.<sup>17,18</sup> Although CAMPs are attractive antimicrobials because of this specificity, they suffer from unresolved issues of systemic toxicity and inflammation, in vivo stability problems, and high production costs.<sup>19</sup> Several groups have attempted to design new types of CAMP mimics to address these disadvantages using small molecules or oligomers that adopt the amphiphilic conformation of CAMPs such as *m*-phenylene ethynylenes (mPE),<sup>20,21</sup> cationic steroid antibiotics (CSA),<sup>22</sup> arylamide foldamers,<sup>23</sup> and synthetic antimicrobial peptidomimetics.<sup>24,25</sup> Although some of these synthetic amphiphilic antimicrobial molecules exhibit good antibacterial activity, most also cause hemolysis.<sup>26</sup> Significantly, no general design principle yet exists for improving the selectivity of membrane targeting in small antimicrobial molecules, and this issue has received little attention.

Considering these issues, we designed new derivatives of  $\alpha$ -mangostin by incorporating cationic groups with different  $\text{pK}_a$  values to tune the amphiphilic properties of the hydrophobic xanthone scaffold and produce compounds with improved selectivity. These new molecules exhibit excellent antibacterial properties, combining the characteristics of  $\alpha$ -mangostin with those of amphiphilic antimicrobial peptides, and exhibit improved hemolysis values ( $\text{HC}_{50}$ ). The most potent of this series of compounds, AM-0016 (**3b**), displays potent antimicrobial properties against a wide range of Gram-positive bacteria including MRSA. AM-0016 (**3b**) kills bacteria rapidly, shows no evidence of resistance or cross-resistance in laboratory assays, and has high biocompatibility. This study provides new insights into the predictive design of synthetic membrane-targeting small molecules with improved selectivity for bacterial membranes over mammalian cell membranes.

## RESULTS AND DISCUSSION

**Chemistry.** A series of xanthone derivatives (**3a–3i**) was designed to test whether functional groups with different  $\text{pK}_a$ s could be used to tune the antimicrobial activity and hemolytic activity of xanthone derivatives to improve their selectivity for bacterial membranes. Amine moieties with high  $\text{pK}_a$  values are more likely to be protonated and develop a cationic charge; therefore, conjugation of these functional groups to the hydrophobic xanthone core would be more likely to result in compounds with amphiphilic properties. Functionalization of the core xanthone molecule was first achieved by the alkylation of two phenolic hydroxyl groups at the C3 and C6 positions of

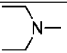
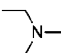
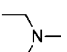
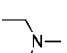
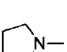
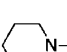
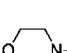
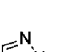
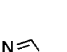
$\alpha$ -mangostin with  $\omega$ -dibromoalkanes using Williamson ether synthesis (Scheme 1). These  $\omega$ -bromoalkyl-substituted compounds act as key intermediates for the further synthesis of cationic xanthone derivatives. The O-alkylated products **2a–2d** were obtained in high yields from 67.1% to 76.5%. It is noteworthy that the hydroxyl group at the C1 position is less reactive because an intramolecular hydrogen bond may form between the C1 hydroxyl group and the C8 carbonyl group.<sup>27</sup> Therefore, we could control the O-alkylation reaction so that it occurred only at the C3 and C6 positions by using mild reaction conditions.<sup>28,29</sup>

To obtain amphiphilic compounds, three types of aliphatic amine (diethylamine, pyrrolidine, and piperidine for compounds **3a–3f**) with high  $\text{pK}_a$  ( $\text{pK}_a = 10.98$ , 11.27, and 11.22, respectively)<sup>30</sup> were chosen to couple with  $\omega$ -bromoalkyl-substituted  $\alpha$ -mangostin. Coupling of the aliphatic amines to  $\omega$ -bromoalkyl-substituted intermediates was carried out in DMSO at room temperature for 4 h, resulting in compounds **3a–3f**, which were obtained with good yields (74.1–91.8%). Alkylation of the secondary amine with alkyl halide is named “Hoffmann alkylation”. The desired alkylation products could be obtained using controlled methods during the synthesis.<sup>31,32</sup> The  $\omega$ -bromoalkyl-substituted xanthone derivatives were treated with a large excess of secondary amines, and the reaction was performed at room temperature. Under these conditions, the tertiary amines were obtained in high yields and no quaternary ammonium salt was isolated.

**Antimicrobial Properties.** Compounds **3a–3f** exhibited excellent antimicrobial activity against clinical isolates of MRSA and *S. aureus* with minimum inhibitory concentrations (MIC) of 0.39–1.56  $\mu\text{g/mL}$  (Table 1), which were superior or comparable to those of  $\alpha$ -mangostin. A rabbit red blood cell hemolysis assay was used as an indicator of mammalian cell selectivity. Of the compounds synthesized, compound **3b** exhibited the best selectivity (50.3). We also investigated the effect of alkyl chain length in the diethylamine-modified compounds **3a–3d**. We found that compounds with longer alkyl chains of  $n = 5$  and 6 (**3c** and **3d**) exhibit slightly reduced antimicrobial activity. Compounds with longer chains are more hydrophobic and tend to aggregate. Therefore, these compounds would have more difficulty in penetrating the peptidoglycan layer of a Gram-positive bacterium.

Next, we investigated the antibacterial activities of **3b** against Gram-negative bacteria. Lipopolysaccharide (LPS) is a major component of the outer membrane in Gram-negative bacteria.<sup>33</sup> A LPS-covered surface acts as a barrier that is less permeable to hydrophobic molecules.<sup>34,35</sup>  $\alpha$ -Mangostin was inactive against Gram-negative bacteria, even at 200  $\mu\text{g/mL}$  (Table 3). In contrast, compound **3b** had moderate antimicrobial activity, with a MIC of 40–50  $\mu\text{g/mL}$  against two strains of Gram-negative bacteria (*Pseudomonas aeruginosa* ATCC27853 and *Klebsiella pneumonia* ATCC10031). This

Table 1. In Vitro Antibacterial Activity (MIC), Hemolytic Properties (HC<sub>50</sub>), and Selectivity of  $\alpha$ -Mangostin Derivatives

Compound	n	R	pKa of conjugated amine, R-H	MIC <sub>99</sub> ( $\mu\text{g mL}^{-1}$ ) <sup>a</sup>		HC <sub>50</sub> <sup>b</sup> ( $\mu\text{g mL}^{-1}$ )	Selectivity (HC <sub>50</sub> /MIC <sub>99</sub> )	
							MRSA	<i>S. aureus</i>
				MRSA	<i>S. aureus</i>			
<b>3a</b>	3		10.98	0.39	0.78	16.3 $\pm$ 2	41.7	20.9
<b>3b</b>	4		10.98	0.39	0.39	19.6 $\pm$ 3	50.3	50.3
<b>3c</b>	5		10.98	0.78	1.56	14.0 $\pm$ 2	18.0	9.00
<b>3d</b>	6		10.98	1.56	1.56	26.5 $\pm$ 2	17.0	17.0
<b>3e</b>	4		11.27	1.56	1.56	25.0 $\pm$ 3	16.0	16.0
<b>3f</b>	4		11.22	1.56	0.78	19.3 $\pm$ 3	12.3	24.7
<b>3g</b>	4		8.36	>200	>200	>200	- <sup>c</sup>	-
<b>3h</b>	4		2.52	>200	>200	>200	-	-
<b>3i</b>	4		2.20	>200	>200	>200	-	-
<b>2b</b>	4	Br	NA <sup>d</sup>	>200	>200	>200	-	-
<b>1</b>	0	H	NA	1.56	1.56	9	5.77	5.77

<sup>a</sup>MRSA: MRSA DM21455, clinical isolate, source: eye; *S. aureus*: *S. aureus* ATCC29213. <sup>b</sup>The HC<sub>50</sub> value was obtained by extrapolating the fitted curve to 50% lysis of red blood cells. <sup>c</sup>The selectivity is undetermined because an exact MIC value was not obtained. <sup>d</sup>Not applicable.

finding demonstrates that appending a cationic charge moiety to a hydrophobic core broadens the antimicrobial spectrum. Djouhri-Bouktab et al. also reported that using positive amine groups to modify squalamine analogues resulted in greater potency against Gram-negative bacteria.<sup>36</sup> Our results clearly demonstrate that the cationic moiety of **3b** is necessary for the compound to bind or form a complex with the negatively charged LPS.

To further confirm that the cationic moieties appended to the hydrophobic xanthone core are necessary to confer

amphiphilic properties for better efficacy and selectivity, we introduced moieties with low pK<sub>a</sub> values, including oxygen- and nitrogen-containing nonaromatic morpholine rings (for **3g**) at C3 and C6 of  $\alpha$ -mangostin. Morpholine is a weak base with a pK<sub>a</sub> of 8.36. We further introduced pyrrole (for **3h**) and 1,2,4-triazole (for **3i**), which contain multiple nitrogens and have an aromatic nature. These two aromatic amines have low pK<sub>a</sub> values (2.52 and 2.20,<sup>37</sup> respectively). Therefore, the nitrogen atoms of **3h** and **3i** are unlikely to be protonated. Synthesis of **3g** (isolated yield = 85.0%) was carried out under the same

conditions as **3a–3f**. However, because the aromatic amines pyrazole and 1,2,4-triazole were less reactive than the aliphatic amines used, the reactions were refluxed in acetone for 48 h. The yields obtained for **3h** and **3i** were 76.8% and 72.4%, respectively.

The results show that **3g**, **3h**, and **3i** are not active against MRSA or *S. aureus* at high concentration (200  $\mu\text{g/mL}$ , Table 1). An intermediate, **2b**, which lacks a cationic moiety, was also inactive against all bacteria, even when tested at 200  $\mu\text{g/mL}$ . Recent reports have also revealed that isoprenyl groups<sup>10</sup> and free C3 and C6 hydroxyl groups<sup>38</sup> play prominent roles in the antimicrobial activity of xanthenes. Thus, the lack of free hydroxyl groups in **3g–3i**, which were conjugated with lower  $\text{pK}_a$  amine moieties, led to a loss of antibacterial activity. However, **3a–3f** also lack free hydroxyl groups at the C3 and C6 positions but remain highly active against Gram-positive bacteria. The results clearly revealed that amphiphilic modifications with amine moieties that have high  $\text{pK}_a$  values are essential to retain and improve antimicrobial activity and selectivity. These results are also supported by a report showing that conjugation of cationic moieties to the relatively hydrophobic benzophenone core is crucial for antibacterial activity against Gram-positive bacteria.<sup>39</sup> We also determined the partition coefficient ( $\log P$ ) values of compounds **1**, **2b**, and **3a–3i** using HPLC methods in accord with The Organisation for Economic Co-operation and Development (OECD) guidelines for the testing of chemicals.<sup>40</sup> We further determined the molecular hydrophobicity of all of the analogues prepared to examine possible correlations of this parameter with antimicrobial activity using a modified method as reported previously.<sup>41,42</sup> The stationary phase of C4-modified silica is hydrophobic and the mobile phase is hydrophilic. When the same HPLC profile was applied, a longer retention time and greater ACN% were measured for compounds with greater molecular hydrophobicity.<sup>41,42</sup> Table 2 shows that the

**Table 2.**  $\log P$  and Hydrophobicity of  $\alpha$ -Mangostin Derivatives

compd	$\log P$	$R_t^a$ (min)	ACN%	MIC <sup>b</sup> ( $\mu\text{g/mL}$ )	HC <sub>50</sub> ( $\mu\text{M}$ )	selectivity
<b>1</b>	6.75	9.87	64.22	1.56	9	5.77
<b>2b</b>	15.01	13.07	83.42	>200	>200	
<b>3a</b>	6.27	8.97	58.82	0.39	16.3	41.7
<b>3b</b>	6.72	9.30	60.80	0.39	19.6	50.3
<b>3c</b>	7.55	9.78	63.68	0.78	14.0	18.0
<b>3d</b>	8.39	10.24	66.40	1.56	26.5	17.0
<b>3e</b>	6.63	9.15	59.90	1.56	25.0	16.0
<b>3f</b>	6.93	9.40	61.40	1.56	19.3	12.3
<b>3g</b>	5.42	8.70	57.20	>200	>200	
<b>3h</b>	9.28	10.81	69.86	>200	>200	
<b>3i</b>	11.08	11.56	74.36	>200	>200	

<sup>a</sup> $R_t$ : retention time. <sup>b</sup>MRSA DM21455, clinical isolate; source: eye.

compounds can be arranged in order of  $\log P$  as follows: **3g** < **3a** < **3e** < **3b** < **1** < **3f** < **3c** < **3d** < **3h** < **3i** < **2b**. Of the analogues with lower  $\log P$  values than  $\alpha$ -mangostin (compound **1**), **3g** does not exhibit antimicrobial properties but compounds **3a**, **3b**, and **3e** exhibit improved antimicrobial properties, HC<sub>50</sub>, and selectivity. Compounds with higher  $\log P$  values than  $\alpha$ -mangostin, such as compounds **3f**, **3c**, and **3d**, exhibited improved antimicrobial properties and selectivity, but compounds **3h**, **3i**, and **2b** were inactive. The molecular

hydrophobicities of the compounds in this series followed a similar trend. Thus,  $\log P$  and molecular hydrophobicity are less predictive than  $\text{pK}_a$  for improving the antimicrobial properties of xanthone analogues.

Encouraged by these results, we screened the antibacterial activity of **3b** against a panel of Gram-positive bacteria (Table

**Table 3.** In Vitro Antibacterial Activity of **1** and **3b** against Gram-Negative Bacteria

Gram-negative strains	MIC ( $\mu\text{g/mL}$ )	
	<b>3b</b>	<b>1</b>
<i>Pseudomonas aeruginosa</i> ATCC27853	50	>200
<i>Klebsiella pneumoniae</i> ATCC10031	40	>200

**Table 4.** MIC Values of **3b** against Gram-positive Bacteria, Including Six Strains of MRSA from Clinical Isolates

Gram-positive strains	MIC	selectivity
MRSA ATCC 700669	0.095	206.3
MRSA DM09808R; source: eye	1.56	12.6
MRSA DB57964/04	0.78	25.1
MRSA DM21595; source: wound	0.39	50.3
MRSA DR42412; source: sputum	0.39	50.3
MRSA DR68004; source: blood	1.56	12.6
VISA 10:DB6506	0.78	25.1
<i>Staphylococcus aureus</i> ATCC29213	0.39	50.3
<i>Staphylococcus aureus</i> ATCC 6538	1.56	12.6
<i>Staphylococcus aureus</i> ATCC 6538P	0.78	25.1
<i>Staphylococcus aureus</i> ATCC 29737	1.56	12.6
<i>Streptococcus faecium</i> ATCC 10541	0.195	100.5
<i>Streptococcus epidermidis</i> ATCC 12228	0.78	25.1
<i>Enterococcus faecalis</i> ATCC 29212	0.78	25.1

4). Compound **3b** exhibited excellent antimicrobial properties against all bacteria tested (MIC = 0.095–1.56  $\mu\text{g/mL}$ ; selectivity index,  $\text{HC}_{50}/\text{MIC}_{99}$  = 12.6–206.3), including three clinical isolates of *S. aureus*, four ATCC strains of *S. aureus*, four clinical isolates of MRSA, one ATCC strain of MRSA, one vancomycin intermediate-resistant (VISA) strain of *S. aureus*, two ATCC strains of *Streptococcus faecium*, and one ATCC strain of *Enterococcus faecalis*. In addition, **3b** also demonstrated comparable or superior antibacterial activities to vancomycin and daptomycin (currently the most widely used antibiotics for MRSA infection) against five selected MRSA strains (Table 5). Compound **3b** was also active against MRSA ATCC700669, a strain with reduced vancomycin sensitivity.<sup>43</sup>

**Table 5.** MIC Values of **3b**, Vancomycin, and Daptomycin against Selected MRSA Strains

bacterial strains	MIC ( $\mu\text{g/mL}$ )		
	<b>3b</b>	daptomycin	vancomycin
MRSA DM21455; source: eye	0.39	0.78	0.78
MRSA DM09808R; source: eye	1.56	0.195	0.39
MRSA DM42412; source: sputum	0.39	0.195	0.78
MRSA ATCC700699 <sup>a</sup>	0.095	0.78	6.25
MRSA DM21595; source: wound	0.39	0.78	0.39

<sup>a</sup>MRSA ATCC700699 exhibits methicillin resistance and reduced vancomycin susceptibility.



Generally, small-molecule antibiotics kill bacteria slowly (over the course of hours),<sup>44</sup> whereas membrane-active amphiphilic antimicrobials and natural antimicrobial peptides are known to kill bacteria rapidly in an hour.<sup>17,36,45</sup> Compound **3b** exhibited concentration-dependent, rapid killing of MRSA, achieving 3-log reductions (99.9% reduction) in viable counts within 5 and 10 min at 2× and 4× MIC, respectively (Figure 1). At 0.5× and 1× MIC, 3-log reductions were achieved in 2 h.

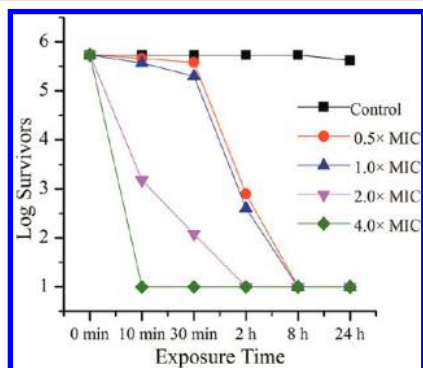


**Figure 1.** Time-kill kinetics of MRSA DM21455 treated with **3b** at various concentrations.

We also compared the time-kill kinetics of **3b** with those of daptomycin and vancomycin against five MRSA strains. Daptomycin achieved a 3-log reduction in approximately 8 h, and vancomycin was only minimally active at 24 h (Figure 2). The rapid time-kill for **3b** demonstrated the advantage of a membrane-directed molecule over vancomycin and daptomycin, which target biosynthetic activities (as well as some membrane properties in the case of daptomycin).<sup>46</sup> The rapid time-kill eliminates the production of subsequent generations of bacteria.

An important characteristic of natural CAMPs is that they have not shown significant amounts of resistance, a problem that is shared among essentially all antibiotics in current use.<sup>47</sup> We simulated the development of resistance using an in vitro multipassage resistance selection study with *S. aureus* and *Enterococcus faecalis* to determine whether spontaneous resistance against **3b** would emerge during prolonged passages at subinhibitory concentrations. Resistance is formally defined as a >4-fold increase in the original MIC.<sup>48</sup> There was no evidence of resistance or cross-resistance against **3b** for any of the four strains tested (Figure 3). Our strategy of modifying  $\alpha$ -mangostin to adopt the amphiphilic topology of CAMPs allowed **3b** to retain the ability to avert resistance like the natural CAMPs<sup>19</sup> and  $\alpha$ -mangostin.<sup>10</sup> Because “dead bugs don’t mutate”,<sup>49</sup> the rapid bactericidal action of **3b** makes this molecule a good candidate for therapeutic use against MRSA.

**Antimicrobial Action.** We recently showed that  $\alpha$ -mangostin, a natural xanthone, appeared to penetrate and disrupt lipid membranes nonselectively, driven by strong hydrophobic forces.<sup>10</sup> In contrast, some amphiphilic molecules, such as CAMPs, may become concentrated on bacterial membranes by electrostatic interaction, disrupting the membrane by interactions between the cationic groups and the negatively charged phosphates, as described by the carpet model.<sup>16</sup> To understand the interaction of **3b** with the bacterial membrane, we investigated the ability of **3b** to depolarize the bacterial membrane using a cytoplasmic membrane-potential-sensitive dye, 3,3'-dipropylthiadicarbocyanine iodide (DiSC<sub>3</sub>-

5).<sup>50</sup> DiSC<sub>3</sub>-5 localizes to the bacterial cytoplasmic membrane, and the fluorescence is self-quenched in the presence of the polarized membrane.<sup>50</sup> The addition of 12.5  $\mu$ g/mL **3b** to a clinical strain of *S. aureus* (DM4001) induced a rapid increase in the fluorescence intensity, indicating that the membrane potential was dissipated (Figure 4). SYTOX Green, a membrane-impermeable cationic cyanine dye, was used to determine whether **3b** disrupts the membrane structure. When the membrane is damaged, the binding of SYTOX Green to nucleic acids will result in an enhanced fluorescence signal.<sup>51,52</sup> Treatment of *S. aureus* DM4001 with 10  $\mu$ M of **3b** and incubation with SYTOX Green led to a rapid rise in fluorescence intensity (Figure 5), which was confirmed by observing the staining of **3b**-treated bacteria using fluorescence microscopy (Figure 6). Large numbers of stained bacteria were observed in a culture incubated with **3b**, clearly indicating that **3b** compromised the living bacterial cytoplasmic membrane. In contrast, membrane permeabilization was not observed in a culture treated with intermediate neutral compound **2b**. Hence, the cationic modification was critical for membrane permeabilization. Morphological changes to *S. aureus* after treatment with **3b** were examined using scanning electron microscopy, as described in our previous report.<sup>10</sup> Structural effects were rapid, and membrane changes were apparent within minutes after incubation of *S. aureus*; these findings agreed well with the results of the time-kill assays. The bacterial membrane exhibited extensive damage, and intracellular components were released (Figure 7). Untreated cells remained as intact spheres with smooth morphology. This shows that **3b** had a profound effect on the bacteria; most membrane depolarizing agents, such as  $\beta$ -defensins (CAMPs)<sup>53</sup> and daptomycin (lipopeptide),<sup>54</sup> have not been shown to induce cell lysis. To develop resistance against membrane-targeting agents such as **3b**, bacteria must change their entire membrane chemistry.<sup>47</sup> This would be very unlikely because it would drastically affect cell viability. The membrane-targeting action of **3b** is expected to play an important role in its rapid time-kill kinetics (Figures 1 and 2) and in minimizing the development of resistance, as shown in the multipassage resistance selection study (Figure 3).

**Molecular Dynamics (MD) Simulations.** MD simulations were used to gain detailed molecular insights into the early events of **3b** membrane targeting using a model of bacterial membranes consisting of 96 POPE and 32 POPG lipids, as constructed by Zhao et al.<sup>55</sup> Consistent with the surface activity model, **3b** had a strong tendency to partition into the bacterial membrane.<sup>16</sup> The high affinity of **3b** for the bacterial membrane arises from electrostatic interactions between the two cationic diethylamine groups and the head groups of anionic lipids, which result in a high surface concentration in the outer leaflet of the membrane. Moreover, the hydrophobicity and, in particular, the planarity of the central xanthone core, further drives **3b** to penetrate deeper into the lipid tail region of the membrane, forming an amphiphilic conformation with the cationic groups located at the hydrophobic–water interface (Figure 8). As a result, this amphiphilic conformation induces large perturbations in the lipid bilayer, including membrane deformation, membrane area expansion, membrane thinning, and enhanced membrane fluctuations (Figure 9). Concomitant with these perturbations, enhanced membrane permeability can be observed in the form of water translocation across the membrane (Figure 8). Because of this permeabilization, membrane organization is disrupted and the membrane becomes leaky. On a longer time scale, these events

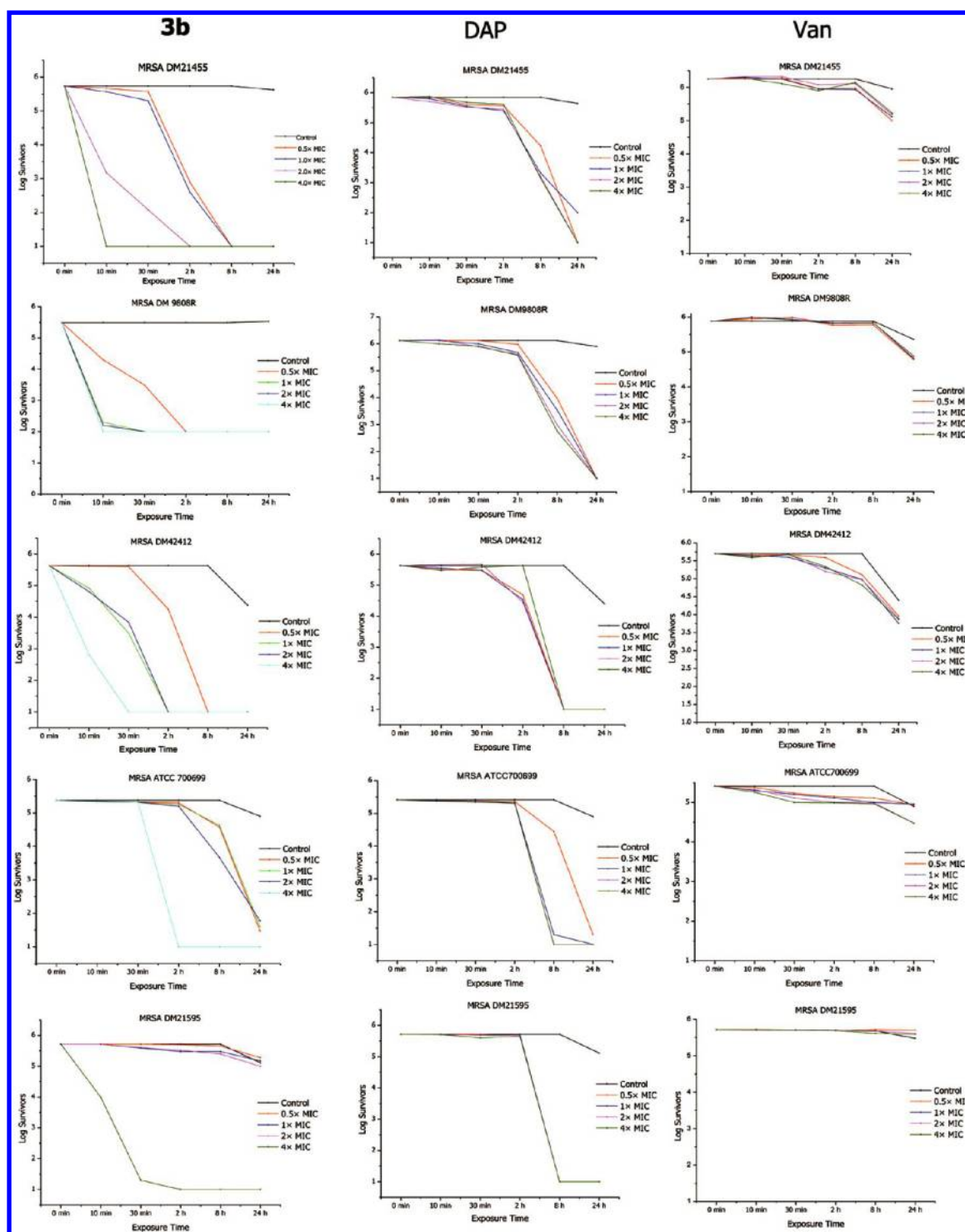


**Figure 2.** Time-kill kinetics of **3b**, daptomycin, and vancomycin tested against five MRSA strains. Abbreviations: Dap, daptomycin; Van, vancomycin.

would likely lead to loss of the membrane potential and cell lysis, resulting in the leaching of intracellular molecules.

Most bacterial membranes contain 20–25% negatively charged phospholipids such as phosphatidylglycerol (PG) and cardiolipin (CL).<sup>56</sup> In contrast, zwitterionic lipids, such as phosphatidylcholine (PC) and sphingomyelin (SM), are the main constituents of the outer leaflets of the mammalian red blood cell membrane.<sup>56</sup> The lower density of negative charges on the mammalian membrane leads to weaker electrostatic interactions with **3b**. Consequently, the surface concentration

of **3b** on the mammalian membrane is much lower. Therefore, this differential interaction appears to be critical to the high selectivity of **3b**. Indeed, the lack of cationicity of  $\alpha$ -mangostin and its resulting inability to discriminate electrostatically between the head groups of bacterial and mammalian membranes accounts for its low selectivity (Figure 10). It is noteworthy that interactions with the head groups of the bacterial membranes restrict **3b** to the hydrophobic–water interface and reduce its penetration into the hydrophobic region of the membrane, resulting in enhanced selectivity.

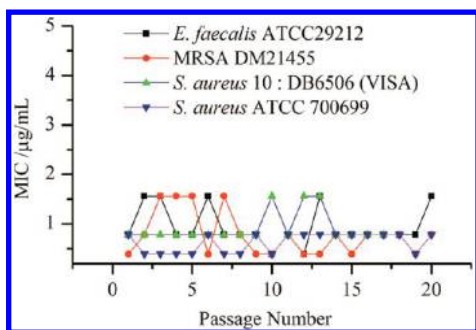


**Figure 3.** Plot of MICs ( $\mu\text{g/mL}$ ) of **3b** against *E. faecalis* ATCC29212, *S. aureus* DM21455 (MRSA), vancomycin intermediate-resistant *S. aureus* (VISA), and *S. aureus* ATCC 700699. No 4-fold increase in MIC was observed in any of the strains tested.

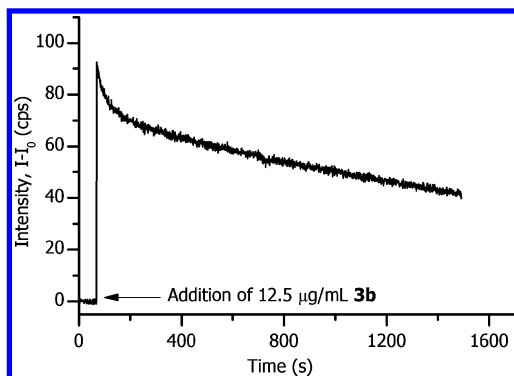


**Figure 4.** Effects of **3b** on the fluorescence intensity of DiSC<sub>3</sub>-5 in the presence of a clinical isolate of *S. aureus*. cps: counts per second.

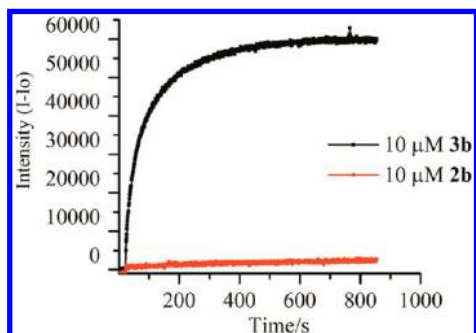


**Figure 5.** Use of the SYTOX Green assay demonstrated that **3b** could induce permeabilization of the bacterial cell membrane. In contrast, no increase in fluorescence was observed when **2b** was added.

Indeed, the inability to interact with these head groups and the rapid lipid solvation convey poor selectivity on  $\alpha$ -mangostin. The MD simulation also revealed that the protonatable moieties with high  $pK_a$  values are crucial for disrupting the bacterial membrane at the hydrophobic–water interface.

**In Vivo Topical Toxicity.** Animals such as mice and rabbits have been widely used in ocular research and toxicity studies due to their easy manipulation, low cost, and biological similarity to humans.<sup>57–59</sup> Although anatomical and physiological differences exist between mice and rabbits, toxicity potential is comparable in both species.<sup>60</sup> Thus, this study was initially conducted to test for potential toxicity to the cornea.

Biocompatibility studies showed that **3b** had no deleterious effects on mouse or rabbit eyes when **3b** was applied topically in PBS. First, initial testing was carried out in the mouse eye,

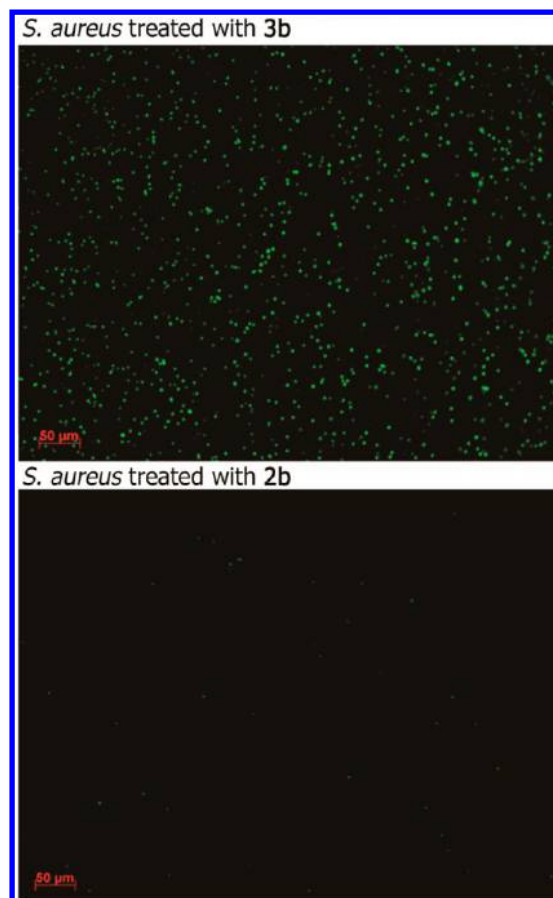


**Figure 6.** Compound **3b** compromised the inner membrane of *S. aureus*. The influx of SYTOX Green and its subsequent binding to nucleic acids caused significant increases in fluorescence emission as indicated by the large number of green-stained bacteria. In contrast, no significant fluorescence emission was observed when bacteria were treated with **2b**.

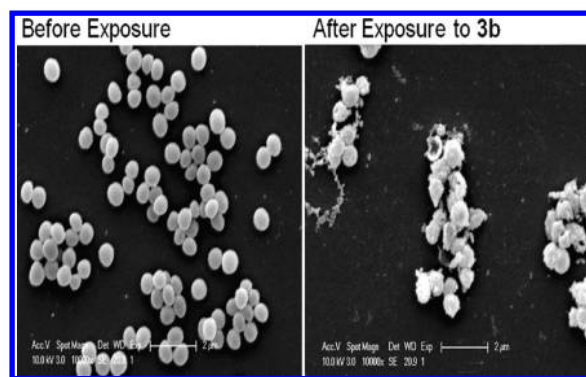


**Figure 7.** Scanning electron micrograph of *S. aureus* DM4001 treated with **3b**, which induced a large amount of membrane leakage after the treatment. In contrast, an untreated culture displayed intact morphology.

using five applications per day at a concentration of 400  $\mu\text{g/mL}$  (S13–1026 $\times$  MIC). Slit lamp photography showed no clinical signs of toxicity or corneal opacity (Figure 11). To further investigate the biocompatibility of **3b**, a corneal epithelial abrasion, 5 mm in diameter, was made by lightly impressing a sterile 5 mm diameter trephine onto the corneal surface, and the epithelium was removed with a mini blade (BD-Beaver) and treated either with saline, vancomycin (50  $\mu\text{g/mL}$ ), or **3b**



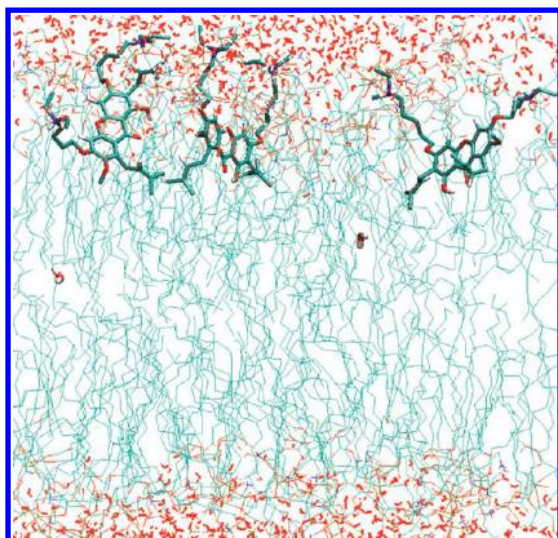


**Figure 8.** MD simulations show that **3b** forms an amphiphilic structure at the membrane–water interface. This perturbs the membrane, allowing water molecules to translocate.

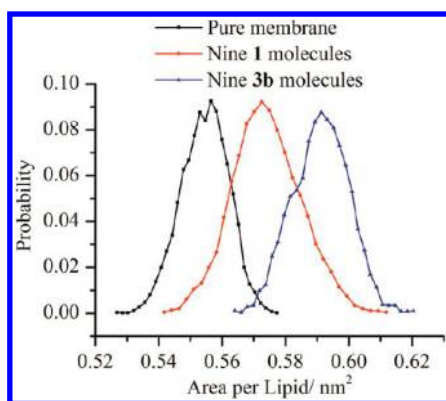


**Figure 9.** Distribution of area per lipid in the bacterial membrane in the presence of nine compound **1** molecules and nine compound **3b** molecules, using 200 ns simulations.

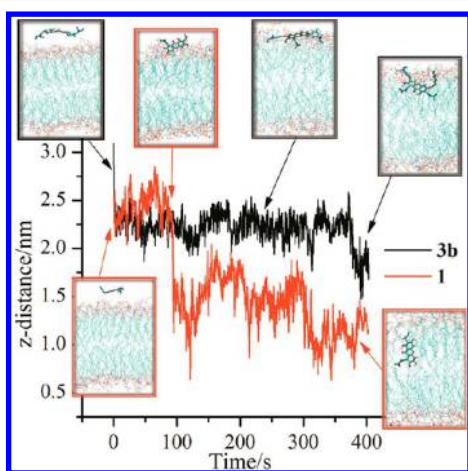


**Figure 10.** Adsorption of one compound **1** (red) molecule and one **3b** (black) molecule onto the simulated bacterial membrane consisting of 128 lipid molecules (DOPE/DOPG = 75/25). The decrease in the drug–membrane distance is an indication of penetration into the membrane. The inset figures show the conformations of compound **1** and compound **3b** at various times.

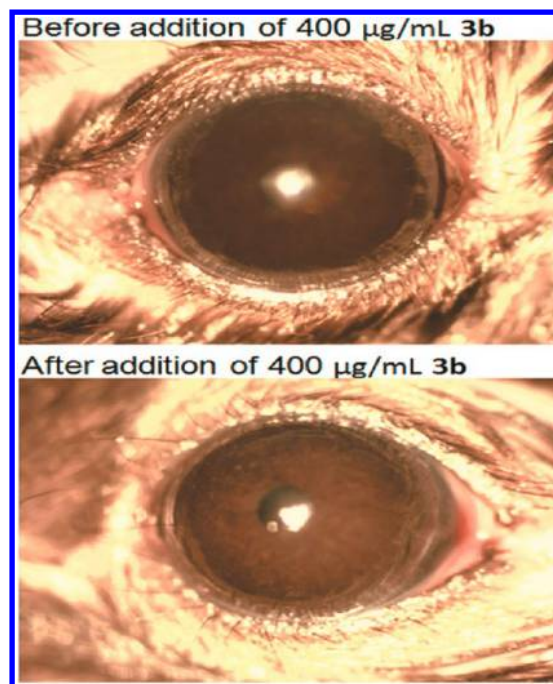


**Figure 11.** Topical application of **3b** onto mouse eyes. Slit lamp photography showed no significant sign of toxicity, and corneal opacity was normal in the treated mice.

(50 µg/mL; 64–128× MIC). The time course of wound closure was determined from fluorescein-stained photographs of the defect size over time. The wound defect area ( $p$  value = 0.376) decreased in both control and treated eyes in a similar manner throughout the healing process (Figure 12). In fact, vancomycin also had no effect on wound healing at this concentration. Short application periods have shown toxicity differences in other studies, in which case the topical drugs resulted in delayed corneal re-epithelialization,<sup>61–63</sup> corneal perforation,<sup>64</sup> and loss of corneal transparency.<sup>65,66</sup> These observations suggest that **3b** offers acceptable biocompatibility with delicate tissues such as the cornea.

**Acute Toxicity Tests.** Studies with animals showed no evidence of toxicity after bolus injection at 50 mg/kg ip and 25 mg/kg iv for 24 h (Table 6). These data are comparable to results for other new antimicrobials such as cathelicidin peptides and those for commercially available antimicrobials such as aminoglycosides and gentamycin.<sup>67–69</sup> Moreover, the excellent bacterial killing efficacy and low MIC values may help to achieve a therapeutic index with significantly low concentration in future clinical development studies.

## CONCLUSIONS

In summary, a series of novel antimicrobials have been designed and prepared by cationic modification of  $\alpha$ -mangostin, a natural xanthone that has a planar hydrophobic core, to yield amphiphilic structures that exhibit improved selectivity for bacterial membranes and disrupt the hydrophobic–water interface. Our results show that the antimicrobial activities of cationic xanthone derivatives can be generally predicted based on the  $pK_a$  values of the corresponding amines. We identified **3b** as the most potent compound in the series. This compound exhibits potent antimicrobial activity against Gram-positive bacteria including MRSA and displays other desirable properties such as improved selectivity, rapid time-kill, avoidance of



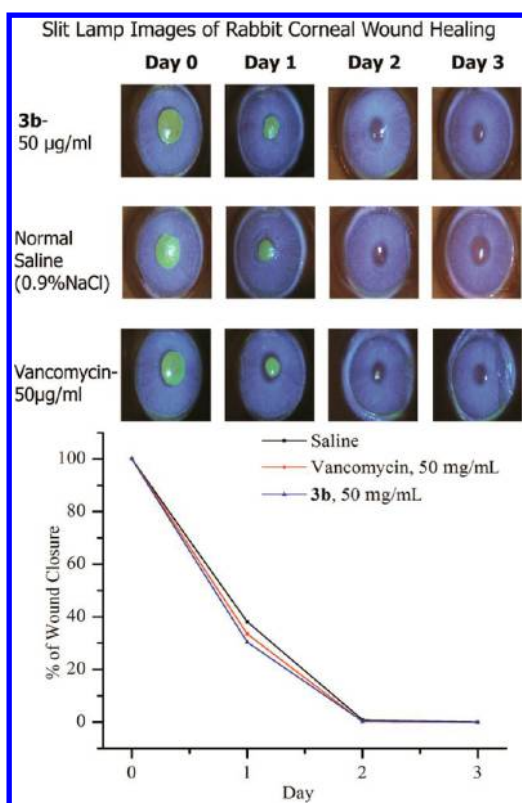


**Figure 12.** Effect of **3b** on wound healing in rabbit cornea. Slit lamp images show that topical application of **3b** at 50 µg/mL on rabbit eyes does not interfere with wound closure. **3b** results in a very similar wound closure percentage as treatment with vancomycin and the control treatment, saline. This shows that **3b** has no toxic effect on corneal wound healing.

**Table 6.** In vivo Acute Toxicity of **3b**: Toxicity Studies using Bolus Injection of **3b** Applied via iv and ip Routes

route	concentration	
	50 mg/kg	25 mg/kg
iv <sup>a</sup>	NT <sup>c</sup>	2/2 <sup>d</sup>
ip <sup>b</sup>	2/2	NT

<sup>a</sup>Intravenous. <sup>b</sup>Intraperitoneal. <sup>c</sup>Not determined. <sup>d</sup>Numbers of animals survived/numbers of animals tested.

antibiotic resistance, and lack of observable in vivo topical toxicity. MD simulation also revealed that **3b** disrupts the bacterial membrane by forming an amphiphilic conformation with cationic groups located at the hydrophobic–water interface. In this study, we have demonstrated a new approach for modifying natural compounds to yield excellent antimicrobial properties, high selectivity, and low toxicity. This strategy could be used to improve the number of “hits” in the development of new antibiotics for drug-resistant pathogens.

## EXPERIMENTAL SECTION

**Chemistry. Materials and Methods.**  $\alpha$ -Mangostin (purity of 99.4%, HPLC) was purchased from Chengdu Biopurify Phytochemicals Ltd. (Chengdu, China). All other starting materials and reagents were purchased from commercial suppliers (Sigma Aldrich, Alfa Aesar, Merck, and Fisher Scientific) and were used without further purification. Column chromatography was carried out with 230–400 mesh silica gel 60 (Merck). TLC analyses were carried out using Merck TLC aluminum sheets (silica gel 60 F<sub>254</sub>). <sup>1</sup>H and <sup>13</sup>C NMR

spectra were recorded using a Bruker Avance 400 MHz with TMS as an internal standard. Chemical shifts are expressed as  $\delta$  values (parts per million, ppm) relative to chloroform ( $\delta$  7.26) for <sup>1</sup>H NMR and chloroform ( $\delta$  77.16) for <sup>13</sup>C NMR. Coupling constants (*J*) are reported in hertz (Hz). Peak multiplicities are reported as singlet (s), doublet (d), triplet (t), quadruplet (q), broad (br), and multiplet (m). ESI mass spectra were measured using an API2000 LC/MS/MS system; APCI mass spectra were measured using a Bruker amaZonX.

**Synthesis and Characterization of 3,6-Di(4-bromobutoxy)-1-hydroxy-7-methoxy-2,8-bis(3-methylbut-2-enyl)-9H-xanthen-9-one (2b).**  $\alpha$ -Mangostin (1.0 g, 2.44 mmol) was dissolved in 15 mL of acetone; then potassium carbonate (1.68 g, 12.20 mmol) and 1, 4-dibromobutane (4.34 mL, 36.6 mmol) were added. The mixture was refluxed for 24 h. After the reaction was complete (as detected by TLC), the solvent was removed under reduced pressure. The oily residue was diluted with EtOAc and washed twice with saturated brine and once with water. The organic phase was dried over anhydrous Na<sub>2</sub>SO<sub>4</sub> and purified via silica gel column chromatography (petroleum ether/EtOAc, 20/1, v/v), affording 1.27 g of product **2b** as a light-yellow solid in 76.5% yield. <sup>1</sup>H NMR (400 MHz, CDCl<sub>3</sub>)  $\delta$  = 13.48 (s, 1H, OH), 6.71 (s, 1H, Ar–H), 6.28 (s, 1H, Ar–H), 5.26–5.19 (m, 2H, 2 × CH), 4.14–4.07 (m, 6H, 3 × CH<sub>2</sub>), 3.80 (s, 3H, OCH<sub>3</sub>), 3.54–3.49 (m, 4H, 2 × CH<sub>2</sub>), 3.35 (d, *J* = 7.2 Hz, 2H, CH<sub>2</sub>), 2.15–2.00 (m, 8H, 4 × CH<sub>2</sub>), 1.85 (s, 3H, CH<sub>3</sub>), 1.79 (s, 3H, CH<sub>3</sub>), 1.68 (s, 6H, 2 × CH<sub>3</sub>). <sup>13</sup>C NMR (101 MHz, CDCl<sub>3</sub>)  $\delta$  = 181.98, 162.54, 159.92, 157.20, 155.24, 155.12, 144.06, 137.38, 131.76, 131.47, 123.22, 122.46, 112.14, 111.55, 104.00, 98.76, 89.19, 67.81, 67.29, 60.91, 33.19, 33.10, 29.39, 29.35, 27.75, 27.60, 26.18, 25.89, 25.80, 21.45, 18.17, 17.86. APCI-MS [*M* + 1] found, 681.2; calculated for C<sub>32</sub>H<sub>40</sub>Br<sub>2</sub>O<sub>6</sub>, 680.5.

**Synthesis and Characterization of 3,6-Di(3-bromopropoxy)-1-hydroxy-7-methoxy-2,8-bis(3-methylbut-2-enyl)-9H-xanthen-9-one (2a).** The compound **2a** was prepared from  $\alpha$ -mangostin (200 mg, 0.487 mmol) and 1,3-dibromopropane (0.74 mL, 7.31 mmol) using the same method as described for **2b**. The product was obtained in 72.3% yield (230 mg) as a light-yellow solid. <sup>1</sup>H NMR (400 MHz, CDCl<sub>3</sub>)  $\delta$  = 13.48 (s, 1H, OH), 6.76 (s, 1H, Ar–H), 6.33 (s, 1H, Ar–H), 5.26–5.19 (m, 2H, 2 × CH), 4.24 (t, 2H, CH<sub>2</sub>), 4.20 (t, 2H, CH<sub>2</sub>), 4.13 (d, *J* = 6.8 Hz, 2H, CH<sub>2</sub>), 3.79 (s, 3H, OCH<sub>3</sub>), 3.68–3.61 (m, 4H, 2 × CH<sub>2</sub>), 3.36 (d, *J* = 6.8 Hz, 2H, CH<sub>2</sub>), 2.46–2.35 (m, 4H, 2 × CH<sub>2</sub>), 1.85 (s, 3H, CH<sub>3</sub>), 1.79 (s, 3H, CH<sub>3</sub>), 1.68 (s, 6H, 2 × CH<sub>3</sub>). <sup>13</sup>C NMR (101 MHz, CDCl<sub>3</sub>)  $\delta$  = 181.99, 162.36, 159.94, 157.01, 155.25, 155.13, 144.04, 137.51, 131.81, 131.50, 123.17, 122.45, 112.30, 111.58, 104.11, 98.95, 89.33, 66.13, 65.78, 60.94, 32.15, 31.84, 29.66, 29.55, 26.18, 25.89, 25.77, 21.45, 18.17, 17.82. APCI-MS [*M* + 1] found, 653.2; calculated for C<sub>30</sub>H<sub>36</sub>Br<sub>2</sub>O<sub>6</sub>, 652.4.

**Synthesis and Characterization of 3,6-Di[(5-bromopentyl)oxy]-1-hydroxy-7-methoxy-2,8-bis(3-methylbut-2-enyl)-9H-xanthen-9-one (2c).** The compound **2c** was prepared from  $\alpha$ -mangostin (411 mg, 1 mmol) and 1,5-dibromopentane (2.06 mL, 15 mmol) using the same method as described for **2b**. The product was obtained in 69.8% yield (495 mg) as a light-yellow solid. <sup>1</sup>H NMR (400 MHz, CDCl<sub>3</sub>)  $\delta$  = 13.49 (s, 1H, OH), 6.71 (s, 1H, Ar–H), 6.28 (s, 1H, Ar–H), 5.26–5.22 (m, 2H, 2 × CH), 4.13 (d, *J* = 6.4 Hz, 2H, CH<sub>2</sub>), 4.09 (t, 2H, CH<sub>2</sub>), 4.05 (t, 2H, CH<sub>2</sub>), 3.80 (s, 3H, OCH<sub>3</sub>), 3.48–3.43 (m, 4H, 2 × CH<sub>2</sub>), 3.36 (d, *J* = 7.2 Hz, 2H, CH<sub>2</sub>), 2.01–1.86 (m, 8H, 4 × CH<sub>2</sub>), 1.85 (s, 3H, CH<sub>3</sub>), 1.80 (s, 3H, CH<sub>3</sub>), 1.74–1.64 (m, 10H, 2 × CH<sub>2</sub>, 2 × CH<sub>3</sub>). <sup>13</sup>C NMR (101 MHz, CDCl<sub>3</sub>)  $\delta$  = 181.98, 162.66, 159.89, 157.31, 155.27, 155.13, 144.06, 137.30, 131.71, 131.37, 123.26, 122.49, 112.04, 111.53, 103.94, 98.71, 89.19, 68.43, 68.02, 60.89, 33.43, 33.40, 32.41, 32.30, 28.31, 28.17, 26.18, 25.89, 25.83, 24.83, 24.81, 21.46, 18.17, 17.84. APCI-MS [*M* + 1] found, 709.2; calculated for C<sub>34</sub>H<sub>44</sub>Br<sub>2</sub>O<sub>6</sub>, 708.5.

**Synthesis and Characterization of 3,6-Di[(6-bromohexyl)oxy]-1-hydroxy-7-methoxy-2,8-bis(3-methylbut-2-enyl)-9H-xanthen-9-one (2d).** The compound **2d** was prepared from  $\alpha$ -mangostin (500 mg, 1.22 mmol) and 1,6-dibromohexane (2.84 mL, 18.3 mmol) using the same method as described for **2b**. The product was obtained in 67.1% yield (602 mg) as a light-yellow oil. <sup>1</sup>H NMR (400 MHz, CDCl<sub>3</sub>)  $\delta$  = 13.49 (s, 1H, OH), 6.70 (s, 1H, Ar–H), 6.28 (s, 1H, Ar–H), 5.26–5.21 (m, 2H, 2 × CH), 4.13 (d, *J* = 6.4 Hz, 2H, CH<sub>2</sub>), 4.08 (t, 2H,

CH<sub>2</sub>), 4.04 (t, 2H, CH<sub>2</sub>), 3.80 (s, 3H, OCH<sub>3</sub>), 3.45–3.42 (m, 4H, 2 × CH<sub>2</sub>), 3.36 (d, *J* = 7.2 Hz, 2H, CH<sub>2</sub>), 1.95–1.86 (m, 8H, 4 × CH<sub>2</sub>), 1.85 (s, 3H, CH<sub>3</sub>), 1.80 (s, 3H, CH<sub>3</sub>), 1.68 (s, 6H, 2 × CH<sub>3</sub>), 1.57–1.52 (m, 8H, 4 × CH<sub>2</sub>). <sup>13</sup>C NMR (101 MHz, CDCl<sub>3</sub>) δ = 181.98, 162.75, 159.86, 157.37, 155.28, 155.18, 144.05, 137.23, 131.68, 131.33, 123.28, 122.51, 111.97, 111.49, 103.93, 98.70, 89.19, 68.56, 68.15, 60.84, 33.67, 33.63, 32.66, 32.57, 28.95, 28.79, 27.87, 27.81, 26.18, 25.90, 25.83, 25.31 (2 × CH<sub>2</sub>), 21.46, 18.17, 17.82. APCI-MS [*M* + 1] found, 737.3; calculated for C<sub>36</sub>H<sub>48</sub>Br<sub>2</sub>O<sub>6</sub>, 736.6.

**Synthesis and Characterization of 3,6-Di[4-(diethylamino)butoxy]-1-hydroxy-7-methoxy-2,8-bis(3-methylbut-2-enyl)-9H-xanthen-9-one (3b).** To a solution of **2b** (100 mg, 0.147 mmol) in DMSO (4 mL), diethylamine (4 mL) was added. The mixture was stirred at room temperature for 4 h. After the reaction was complete, the mixture was diluted with 50 mL of ethyl acetate and then washed with aqueous NaHCO<sub>3</sub> and saturated brine (each three times). The organic phase was dried over anhydrous Na<sub>2</sub>SO<sub>4</sub> and concentrated under a vacuum. The residual crude oil was purified via silica gel column chromatography (EtOAc/MeOH/Et<sub>3</sub>N, 100/2/1, v/v), producing 80.8 mg of pure product **3b** as a yellow oil in 82.7% yield. <sup>1</sup>H NMR (400 MHz, CDCl<sub>3</sub>) δ = 13.50 (s, 1H, OH), 6.72 (s, 1H, Ar–H), 6.29 (s, 1H, Ar–H), 5.26–5.23 (m, 2H, 2 × CH), 4.13 (d, *J* = 7.2 Hz, 2H, CH<sub>2</sub>), 4.10 (t, 2H, CH<sub>2</sub>), 4.06 (t, 2H, CH<sub>2</sub>), 3.80 (s, 3H, OCH<sub>3</sub>), 3.36 (d, *J* = 7.2 Hz, 2H, CH<sub>2</sub>), 2.59–2.51 (m, 12H, 6 × CH<sub>2</sub>), 1.95–1.82 (m, 7H, 2 × CH<sub>2</sub>, 1 × CH<sub>3</sub>), 1.80 (s, 3H, CH<sub>3</sub>), 1.73–1.64 (m, 10H, 2 × CH<sub>2</sub>, 2 × CH<sub>3</sub>), 1.04 (t, 12H, 4 × CH<sub>3</sub>). <sup>13</sup>C NMR (101 MHz, CDCl<sub>3</sub>) δ = 182.01, 162.77, 159.86, 157.41, 155.31, 155.17, 144.06, 137.20, 131.68, 131.35, 123.31, 122.51, 111.96, 111.49, 103.90, 98.75, 89.23, 68.75, 68.32, 60.84, 52.46, 52.45, 46.82 (2 × CH<sub>2</sub>), 46.79 (2 × CH<sub>2</sub>), 27.26, 27.09, 26.19, 25.91, 25.83, 23.63, 23.44, 21.47, 18.18, 17.84, 11.55 (2 × CH<sub>3</sub>), 11.54 (2 × CH<sub>3</sub>). ESI-MS [*M* + 1] found, 665.2; calculated for C<sub>40</sub>H<sub>60</sub>N<sub>2</sub>O<sub>6</sub>, 664.9.

**Synthesis and Characterization of 3,6-Di[3-(diethylamino)propoxy]-1-hydroxy-7-methoxy-2,8-bis(3-methylbut-2-enyl)-9H-xanthen-9-one (3a).** The compound **3a** was prepared from **2a** (100 mg, 0.153 mmol) and diethylamine (4 mL) using the same method as described for **3b**. The product was obtained in 83.2% yield (81.2 mg) as a yellow oil. <sup>1</sup>H NMR (400 MHz, CDCl<sub>3</sub>) δ = 13.51 (s, 1H, OH), 6.75 (s, 1H, Ar–H), 6.32 (s, 1H, Ar–H), 5.26–5.23 (m, 2H, 2 × CH), 4.16–4.09 (m, 6H, 3 × CH<sub>2</sub>), 3.80 (s, 3H, OCH<sub>3</sub>), 3.36 (d, *J* = 6.8 Hz, 2H, CH<sub>2</sub>), 2.70–2.65 (m, 4H, 2 × CH<sub>2</sub>), 2.61–2.56 (m, 8H, 4 × CH<sub>2</sub>), 2.06–1.97 (m, 4H, 2 × CH<sub>2</sub>), 1.85 (s, 3H, CH<sub>3</sub>), 1.79 (s, 3H, CH<sub>3</sub>), 1.67 (s, 6H, 2 × CH<sub>3</sub>), 1.05 (t, 12H, 4 × CH<sub>3</sub>). <sup>13</sup>C NMR (101 MHz, CDCl<sub>3</sub>) δ = 182.03, 162.76, 159.84, 157.43, 155.33, 155.18, 144.03, 137.18, 131.67, 131.37, 123.32, 122.58, 111.97, 111.46, 103.92, 98.82, 89.28, 67.25, 66.78, 60.83, 49.46, 49.38, 47.10 (2 × CH<sub>2</sub>), 47.02 (2 × CH<sub>2</sub>), 26.98, 26.80, 26.19, 25.91, 25.80, 21.45, 18.18, 17.89, 11.70 (2 × CH<sub>3</sub>), 11.65 (2 × CH<sub>3</sub>). ESI-MS [*M* + 1] found, 636.9; calculated for C<sub>38</sub>H<sub>56</sub>N<sub>2</sub>O<sub>6</sub>, 636.9.

**Synthesis and Characterization of 3,6-Di[5-(diethylamino)pentyl]oxy]-1-hydroxy-7-methoxy-2,8-bis(3-methylbut-2-enyl)-9H-xanthen-9-one (3c).** The compound **3c** was prepared from **2c** (110 mg, 0.155 mmol) and diethylamine (4 mL) using the same method as described for **3b**. The product was obtained in 91.8% yield (98.8 mg) as a yellow oil. <sup>1</sup>H NMR (400 MHz, CDCl<sub>3</sub>) δ = 13.50 (s, 1H, OH), 6.70 (s, 1H, Ar–H), 6.28 (s, 1H, Ar–H), 5.26–5.23 (m, 2H, 2 × CH), 4.13 (d, *J* = 6.4 Hz, 2H, CH<sub>2</sub>), 4.07 (t, 2H, CH<sub>2</sub>), 4.03 (t, 2H, CH<sub>2</sub>), 3.80 (s, 3H, OCH<sub>3</sub>), 3.36 (d, *J* = 6.8 Hz, 2H, CH<sub>2</sub>), 2.56–2.50 (m, 8H, 4 × CH<sub>2</sub>), 2.46–2.43 (t, 4H, 2 × CH<sub>2</sub>), 1.94–1.86 (m, 4H, 2 × CH<sub>2</sub>), 1.84 (s, 3H, CH<sub>3</sub>), 1.79 (s, 3H, CH<sub>3</sub>), 1.67 (s, 6H, 2 × CH<sub>3</sub>), 1.54–1.49 (m, 8H, 4 × CH<sub>2</sub>), 1.02 (t, 12H, 4 × CH<sub>3</sub>). <sup>13</sup>C NMR (101 MHz, CDCl<sub>3</sub>) δ = 182.00, 162.83, 159.84, 157.43, 155.30, 155.16, 144.06, 137.15, 131.64, 131.26, 123.34, 122.55, 111.92, 111.48, 103.86, 98.70, 89.22, 68.74, 68.33, 60.82, 52.90, 52.84, 46.91 (4 × CH<sub>2</sub>), 29.14, 28.96, 26.88 (2 × CH<sub>2</sub>), 26.18, 25.90, 25.83, 24.20 (2 × CH<sub>2</sub>), 21.47, 18.17, 17.82, 11.67 (4 × CH<sub>3</sub>). ESI-MS [*M* + 1] found, 693.4; calculated for C<sub>42</sub>H<sub>64</sub>N<sub>2</sub>O<sub>6</sub>, 693.0.

**Synthesis and Characterization of 3,6-Di[6-(diethylamino)hexyl]oxy]-1-hydroxy-7-methoxy-2,8-bis(3-methylbut-2-enyl)-9H-xanthen-9-one (3d).** The compound **3d** was prepared from **2d** (100 mg, 0.136 mmol) and diethylamine (4 mL) using the same method as

described for **3b**. The product was obtained in 77.8% yield (76.1 mg) as a yellow oil. <sup>1</sup>H NMR (400 MHz, CDCl<sub>3</sub>) δ = 13.50 (s, 1H, OH), 6.71 (s, 1H, Ar–H), 6.29 (s, 1H, Ar–H), 5.26–5.23 (m, 2H, 2 × CH), 4.13 (d, *J* = 6.4 Hz, 2H, CH<sub>2</sub>), 4.07 (t, 2H, CH<sub>2</sub>), 4.03 (t, 2H, CH<sub>2</sub>), 3.80 (s, 3H, OCH<sub>3</sub>), 3.36 (d, *J* = 7.2 Hz, 2H, CH<sub>2</sub>), 2.57–2.51 (m, 8H, 4 × CH<sub>2</sub>), 2.46–2.42 (m, 4H, 2 × CH<sub>2</sub>), 1.94–1.79 (m, 10H, 2 × CH<sub>2</sub>, 2 × CH<sub>3</sub>), 1.67 (s, 6H, 2 × CH<sub>3</sub>), 1.58–1.47 (m, 8H, 4 × CH<sub>2</sub>), 1.42–1.35 (m, 4H, 2 × CH<sub>2</sub>), 1.03 (t, 12H, 4 × CH<sub>3</sub>). <sup>13</sup>C NMR (101 MHz, CDCl<sub>3</sub>) δ = 182.01, 162.85, 159.85, 157.46, 155.31, 155.17, 144.06, 137.17, 131.67, 131.30, 123.32, 122.52, 111.92, 111.49, 103.87, 98.71, 89.23, 68.76, 68.38, 60.83, 52.87, 52.84, 46.89 (4 × CH<sub>2</sub>), 29.11, 28.93, 27.44, 27.36, 26.92 (2 × CH<sub>2</sub>), 26.19, 26.10, 26.09, 25.91, 25.85, 21.48, 18.18, 17.82, 11.56 (4 × CH<sub>3</sub>). ESI-MS [*M* + 1] found, 722.4; calculated for C<sub>44</sub>H<sub>68</sub>N<sub>2</sub>O<sub>6</sub>, 721.0.

**Synthesis and Characterization of 1-Hydroxy-7-methoxy-2,8-bis(3-methylbut-2-enyl)-3,6-di[4-(1-pyrrolidinyl)butoxy]-9H-xanthen-9-one (3e).** The compound **3e** was prepared from **2b** (100 mg, 0.147 mmol) and pyrrolidine (4 mL) using the same method as described for **3b**. The product was obtained in 78.1% yield (75.8 mg) as a yellow oil. <sup>1</sup>H NMR (400 MHz, CDCl<sub>3</sub>) δ = 13.49 (s, 1H, OH), 6.72 (s, 1H, Ar–H), 6.29 (s, 1H, Ar–H), 5.26–5.22 (m, 2H, 2 × CH), 4.14–4.04 (m, 6H, 3 × CH<sub>2</sub>), 3.80 (s, 3H, OCH<sub>3</sub>), 3.36 (d, *J* = 6.8 Hz, 2H, CH<sub>2</sub>), 2.57–2.52 (m, 12H, 6 × CH<sub>2</sub>), 1.99–1.72 (m, 22H, 8 × CH<sub>2</sub>, 2 × CH<sub>3</sub>), 1.67 (s, 6H, 2 × CH<sub>3</sub>). <sup>13</sup>C NMR (101 MHz, CDCl<sub>3</sub>) δ = 181.99, 162.74, 159.60, 156.98, 155.28, 155.14, 144.03, 137.17, 131.65, 131.33, 123.30, 122.51, 111.93, 111.47, 103.88, 98.73, 89.21, 68.68, 68.22, 60.84, 56.08, 56.02, 54.17 (2 × CH<sub>2</sub>), 54.16 (2 × CH<sub>2</sub>), 27.23, 27.06, 26.17, 25.89, 25.81, 25.51, 25.48, 23.41 (4 × CH<sub>3</sub>), 21.45, 18.16, 17.83. ESI-MS [*M* + 1] found, 661.2; calculated for C<sub>40</sub>H<sub>56</sub>N<sub>2</sub>O<sub>6</sub>, 660.9.

**Synthesis and Characterization of 1-Hydroxy-7-methoxy-2,8-bis(3-methylbut-2-enyl)-3,6-di[4-(1-piperidinyl)butoxy]-9H-xanthen-9-one (3f).** The compound **3f** was prepared from **2b** (100 mg, 0.147 mmol) and piperidine (4 mL) using the same method as described for **3b**. The product was obtained in 74.1% yield (75.0 mg) as a yellow oil. <sup>1</sup>H NMR (400 MHz, CDCl<sub>3</sub>) δ = 13.50 (s, 1H, OH), 6.73 (s, 1H, Ar–H), 6.29 (s, 1H, Ar–H), 5.26–5.23 (m, 2H, 2 × CH), 4.13 (d, *J* = 6.8 Hz, 2H, CH<sub>2</sub>), 4.10 (t, 2H, CH<sub>2</sub>), 4.05 (t, 2H, CH<sub>2</sub>), 3.80 (s, 3H, OCH<sub>3</sub>), 3.36 (d, *J* = 7.2 Hz, 2H, CH<sub>2</sub>), 2.40–2.36 (m, 12H, 6 × CH<sub>2</sub>), 1.95–1.82 (m, 7H, 2 × CH<sub>2</sub>, 1 × CH<sub>3</sub>), 1.79 (s, 3H, CH<sub>3</sub>), 1.76–1.71 (m, 4H, 2 × CH<sub>2</sub>), 1.67 (s, 6H, 2 × CH<sub>3</sub>), 1.62–1.57 (m, 8H, 4 × CH<sub>2</sub>), 1.45–1.39 (m, 4H, 2 × CH<sub>2</sub>). <sup>13</sup>C NMR (101 MHz, CDCl<sub>3</sub>) δ = 182.01, 162.78, 159.86, 157.41, 155.31, 155.17, 144.06, 137.19, 131.66, 131.34, 123.33, 122.53, 111.94, 111.50, 103.89, 98.75, 89.23, 68.73, 68.32, 60.85, 59.00, 58.89, 54.63 (2 × CH<sub>2</sub>), 54.60 (2 × CH<sub>2</sub>), 27.29, 27.10, 26.19, 25.97 (4 × CH<sub>2</sub>), 25.91, 25.82, 24.48 (2 × CH<sub>2</sub>), 23.44 (2 × CH<sub>2</sub>), 21.47, 18.18, 17.85. ESI-MS [*M* + 1] found, 689.1; calculated for C<sub>42</sub>H<sub>60</sub>N<sub>2</sub>O<sub>6</sub>, 688.9.

**Synthesis and Characterization of 1-Hydroxy-7-methoxy-2,8-bis(3-methylbut-2-enyl)-3,6-di(4-morpholinobutoxy)-9H-xanthen-9-one (3g).** The compound **3g** was prepared from **2b** (100 mg, 0.147 mmol) and morpholine (4 mL) using the same method as described for **3b**. The product was obtained in 85.0% yield (86.6 mg) as a yellow oil. <sup>1</sup>H NMR (400 MHz, CDCl<sub>3</sub>) δ = 13.49 (s, 1H, OH), 6.73 (s, 1H, Ar–H), 6.30 (s, 1H, Ar–H), 5.25–5.22 (m, 2H, 2 × CH), 4.14–4.05 (m, 6H, 3 × CH<sub>2</sub>), 3.80 (s, 3H, OCH<sub>3</sub>), 3.74–3.71 (m, 8H, 4 × CH<sub>2</sub>), 3.36 (d, *J* = 6.8 Hz, 2H, CH<sub>2</sub>), 2.46–2.41 (m, 12H, 6 × CH<sub>2</sub>), 1.98–1.87 (m, 4H, 2 × CH<sub>2</sub>), 1.85 (s, 3H, CH<sub>3</sub>), 1.79 (s, 3H, CH<sub>3</sub>), 1.77–1.69 (m, 4H, 2 × CH<sub>2</sub>), 1.67 (s, 6H, 2 × CH<sub>3</sub>). <sup>13</sup>C NMR (101 MHz, CDCl<sub>3</sub>) δ = 181.99, 162.73, 159.90, 157.37, 155.29, 155.16, 144.07, 137.30, 131.72, 131.37, 123.27, 122.51, 112.01, 111.51, 103.92, 98.75, 89.20, 68.62, 68.19, 66.97 (2 × CH<sub>2</sub>), 66.95 (2 × CH<sub>2</sub>), 60.85, 58.52, 58.41, 53.71 (4 × CH<sub>2</sub>), 27.05, 26.86, 26.19, 25.90, 25.82, 23.03 (2 × CH<sub>2</sub>), 21.47, 18.18, 17.84. ESI-MS [*M* + 1] found, 693.3; calculated for C<sub>40</sub>H<sub>56</sub>N<sub>2</sub>O<sub>8</sub>, 692.9.

**Synthesis and Characterization of 3,6-Di[4-(1-pyrazolyl)butoxy]-1-hydroxy-7-methoxy-2,8-bis(3-methylbut-2-enyl)-9H-xanthen-9-one (3h).** To a solution of **2b** (100 mg, 0.147 mmol) in acetone (4 mL), 1H-pyrazole (100 mg, 1.47 mmol) and potassium carbonate (101 mg, 0.735 mmol) were added. The mixture was refluxed for 48 h. After the reaction was complete, the solvent was removed under



reduced pressure. The residue was diluted with 50 mL of ethyl acetate and washed three times with saturated brine, and then dried over anhydrous  $\text{Na}_2\text{SO}_4$ . After removal of the solvent, the residual mixture was purified via silica gel column chromatography ( $\text{EtOAc}/\text{MeOH}/\text{Et}_3\text{N}$ , 100/2/1, v/v), producing 73.9 mg of product **3h** as a light-yellow solid in 76.8% yield.  $^1\text{H}$  NMR (400 MHz,  $\text{CDCl}_3$ )  $\delta$  = 13.48 (s, 1H, OH), 7.52 (m, 2H, Ar-H), 7.42 (d,  $J$  = 2.0 Hz, 1H, Ar-H), 7.40 (d,  $J$  = 2.4 Hz, 1H, Ar-H), 6.68 (s, 1H, Ar-H), 6.26–6.25 (m, 3H, 3  $\times$  Ar-H), 5.25–5.19 (m, 2H, 2  $\times$  CH), 4.27–4.21 (m, 4H, 2  $\times$   $\text{CH}_2$ ), 4.12 (d,  $J$  = 6.4 Hz, 2H,  $\text{CH}_2$ ), 4.08–4.01 (m, 4H, 2  $\times$   $\text{CH}_2$ ), 3.78 (s, 3H,  $\text{OCH}_3$ ), 3.35 (d,  $J$  = 7.2 Hz, 2H,  $\text{CH}_2$ ), 2.16–2.06 (m, 4H, 2  $\times$   $\text{CH}_2$ ), 1.92–1.77 (m, 10H, 2  $\times$   $\text{CH}_2$ , 2  $\times$   $\text{CH}_3$ ), 1.68 (s, 6H, 2  $\times$   $\text{CH}_3$ ).  $^{13}\text{C}$  NMR (101 MHz,  $\text{CDCl}_3$ )  $\delta$  = 181.96, 162.52, 159.87, 157.18, 155.23, 155.10, 144.02, 139.33, 139.24, 137.30, 131.71, 131.40, 128.98, 128.86, 123.22, 122.47, 112.06, 111.46, 105.47, 105.44, 103.95, 98.77, 89.20, 68.11, 67.63, 60.88, 51.60, 51.52, 27.22, 27.17, 26.26, 26.16, 26.11, 25.88, 25.77, 21.44, 18.16, 17.82. ESI-MS [ $M+1$ ] found, 655.2; calculated for  $\text{C}_{38}\text{H}_{46}\text{N}_4\text{O}_6$ , 654.8.

**Synthesis and Characterization of 3,6-Di[4-(1–1,2,4-triazolyl)-butoxy]-1-hydroxy-7-methoxy-2,8-bis(3-methylbut-2-enyl)-9H-xanthen-9-one (**3i**).** The compound **3i** was prepared from **2b** (100 mg, 0.147 mmol) and 1H-1,2,4-triazole (101 mg, 1.47 mmol) using the same method as described for **3h**. The product was obtained in 72.4% yield (69.9 mg) as a light-yellow solid.  $^1\text{H}$  NMR (400 MHz,  $\text{CDCl}_3$ )  $\delta$  = 13.47 (s, 1H, OH), 8.13 (s, 1H, Ar-H), 8.08 (s, 1H, Ar-H), 7.96 (s, 2H, Ar-H), 6.69 (s, 1H, Ar-H), 6.26 (s, 1H, Ar-H), 5.26–5.18 (m, 2H, 2  $\times$  CH), 4.33–4.26 (m, 4H, 2  $\times$   $\text{CH}_2$ ), 4.13–4.05 (m, 6H, 3  $\times$   $\text{CH}_2$ ), 3.79 (s, 3H,  $\text{OCH}_3$ ), 3.35 (d,  $J$  = 6.8 Hz, 2H,  $\text{CH}_2$ ), 2.20–2.10 (m, 4H, 2  $\times$   $\text{CH}_2$ ), 1.94–1.86 (m, 4H, 2  $\times$   $\text{CH}_2$ ), 1.84 (s, 3H,  $\text{CH}_3$ ), 1.77 (s, 3H,  $\text{CH}_3$ ), 1.68 (s, 3H,  $\text{CH}_3$ ), 1.65 (s, 3H,  $\text{CH}_3$ ).  $^{13}\text{C}$  NMR (101 MHz,  $\text{CDCl}_3$ )  $\delta$  = 181.96, 162.40, 159.98, 157.08, 155.24, 155.11, 152.14, 152.09, 144.05, 143.07, 142.91, 137.54, 131.86, 131.56, 123.15, 122.43, 112.25, 111.53, 104.06, 98.81, 89.19, 68.05, 67.46, 60.95, 49.26, 49.15, 26.92, 26.76, 26.20, 26.15, 25.95, 25.90, 25.79, 21.47, 18.19, 17.85. ESI-MS [ $M+1$ ] found, 657.4; calculated for  $\text{C}_{36}\text{H}_{44}\text{N}_6\text{O}_6$ , 656.8.

**Bacterial Strains and Growth Conditions.** The bacterial strains used in these studies were *Staphylococcus aureus* ATCC29213, *S. aureus* ATCC6538, *S. aureus* ATCC6538P, *S. aureus* ATCC29737, MRSA ATCC700699, *E. faecalis* ATCC29212, *Streptococcus faecium* ATCC10541, *S. epidermidis* (ATCC12228), *Pseudomonas aeruginosa* ATCC27853, *Klebsiella pneumoniae* ATCC10031 and the following clinical isolates: *S. aureus* DM4001 (from eye), *S. aureus* DM4400R (from cornea), *S. aureus* DM4583R, *S. aureus* 10:DB6506 (VISA), MRSA DM57964/04, MRSA DM21455 (from eye), DM09808R (from eye), MRSA DM21595 (from wound), MRSA DR42412 (from sputum), and MRSA DR68004 (from blood). The direct colony suspension method prescribed by the Clinical and Laboratory Standards Institute (CLSI) was used for inoculum preparation. Inoculum suspensions were prepared from isolated colonies selected from an 18- to 20-h Tryptic Soy Agar (TSA) plate.

**Susceptibility Testing.** MIC determinations for **3b** were performed in Mueller–Hinton broth (MHB) using broth macrodilution following CLSI guidelines. Compounds **1**, **2**, and **3a–3i** were first dissolved in *N,N*-dimethylformamide (DMF) to make 1000  $\mu\text{g}/\text{mL}$  stock solutions. Serial 2-fold dilutions of the compounds were prepared in cation-adjusted MHB in test tubes. The concentration of the above-mentioned inoculum suspension was adjusted in MHB. After inoculation, each tube contained approximately  $5 \times 10^5$  colony forming units (CFU)/mL. The tubes were then incubated for 20–22 h at 35  $^\circ\text{C}$ . The strains used in susceptibility testing are listed in Tables 1, 3, 4, and 5. The MIC of daptomycin (Tocris Bioscience) was measured in MHB supplemented with 50 mg/mL free  $\text{Ca}^{2+}$ . Vancomycin was first dissolved in sterile water to prepare a 1000  $\mu\text{g}/\text{mL}$  stock solution. Then, the MIC was determined using the broth macrodilution method, as mentioned above. Vancomycin was the second ASEAN Reference Standard (ARS) and was obtained from the representative of ARS Singapore.

**Hemolysis Assay.** The hemolytic activity of antimicrobials was determined by the amount of hemoglobin released from rabbit

erythrocytes based on a modified method.<sup>70</sup> Fresh rabbit red blood cells (RBCs) were isolated from the whole blood of New Zealand white rabbits. The procedures used were approved by the IACUC of SingHealth and performed according to the standards of the Association for Research in Vision and Ophthalmology. The RBCs were centrifuged at 3000 rpm for 10 min and then washed twice with sterile PBS. Compounds **1**, **2b**, **3g**, **3h**, and **3i** were dissolved in DMSO. Compounds **3a–3e** were dissolved in PBS. The solutions were mixed with RBCs to prepare the desired concentration (final v/v = 4%). The final DMSO concentration in each mixture was <1% to ensure that the DMSO had a negligible effect on hemolytic activity. The mixtures were added to 96-well plates and incubated at 37  $^\circ\text{C}$  for 60 min. After incubation, the mixtures were transferred to 1.5 mL Eppendorf tubes and centrifuged at 3000 rpm for 3 min. The supernatant (100  $\mu\text{L}$ ) was transferred to a clean 96-well plate, and the amount of hemoglobin released was determined by measuring the absorbance (abs) at 576 nm using a TECAN Infinite 200 microplate reader. A solution of 2% Triton X-100 was used as a positive control. PBS and 1% DMSO were used as negative controls. Percent of hemolysis was calculated using the following equation:

$$\% \text{hemolysis} = \frac{\text{mixture abs}_{576\text{nm}} - \text{negative control abs}_{576\text{nm}}}{\text{positive control abs}_{576\text{nm}} - \text{negative control abs}_{576\text{nm}}} \times 100$$

**Molecular Hydrophobicity Analysis.** The molecular hydrophobicities of the synthesized analogues were characterized in terms of retention time and ACN% using an HPLC (Waters 2695 separation module) equipped with a Waters Delta-Pak CA 300  $\text{\AA}$  column. The experiments were conducted under the same conditions for all analogues. The samples were injected at 10  $\mu\text{g}/\text{mL}$ , with an injection volume of 20  $\mu\text{L}$  and a flow rate of 1 mL/min. The gradient profile was 5–95% over 15 min.

**Time-Kill Studies.** The bacterial strains used in the time-kill studies (MRSA DM21455, MRSA DM09808R, MRSA DM42412, MRSA 21595, and MRSA ATCC700699) were picked from isolated colonies on an 18–20 h tryptic soy agar (TSA) plate. The inoculums were suspended and adjusted in 0.31 mM phosphate buffer to obtain a bacterial suspension with  $10^5$  to  $10^6$  CFU/mL. The inoculum was then treated with various concentrations (0.5 $\times$ , 1 $\times$ , 2 $\times$ , and 4 $\times$  MIC) of **3b**, daptomycin, and vancomycin. The mixtures were incubated at 35  $^\circ\text{C}$ . Culture aliquots were removed at 10 min, 30 min, 2 h, 8 h, and 24 h to measure viable plate counts. The aliquots were diluted serially 10-fold using D/E neutralization broth, and 20  $\mu\text{L}$  of each dilution was plated on TSA plates using the surface-spread plate method. The plates were then incubated at 35  $^\circ\text{C}$  for 48–72 h. Bacterial viability was determined by counting the colonies grown on the plates. Bactericidal activity was defined as a 3-log reduction of viable count in cultures treated with an antimicrobial compound compared to an untreated control. The detection limit for a reliable plate count was 100 CFU/mL for **3b** against MRSA DM09808R and 10 CFU/mL for all other time-kill studies.

**Multipassage Resistance Selection Studies.** Multipassage resistance selection studies were performed using **3b** with *E. faecalis* ATCC29212, MRSA DM21455, *S. aureus* 10:DB6506 (VISA), and *S. aureus* ATCC 700699. A 2-fold dilution series of eight concentrations of **3b** from 50  $\mu\text{g}/\text{mL}$  was prepared. The resistance of the strains against **3b** was determined based on the progressive increase in the MIC of the bacteria over several passages. Bacterial growth in each dilution was examined after 20 to 22 h of incubation. Bacteria that grew in 0.5 $\times$  of the MIC of **3b** were repassaged in a fresh dilution series of eight concentrations. **3b** was repassaged for at least 17 passages in each culture. In this study, resistance was defined as an increase in the initial MIC of more than 4-fold.<sup>48</sup>

**Cytoplasmic Membrane Depolarization Assay.** 3,3'-Dipropylthiadicarbocyanide iodide ( $\text{DiSC}_3-5$ ) is a membrane-potential-sensitive probe. Partitioning of  $\text{DiSC}_3-5$  onto the polarized cytoplasmic membrane self-quenches the fluorescence intensity. Addition of a membrane-active antimicrobial that dissipates the membrane potential



leads to the release of  $\text{DiSC}_3\text{-S}$ , and the resulting increase in fluorescence can be observed and monitored. The effect of **3b** on the membrane potential of the isolate *S. aureus* (DM4001) was investigated using a modified version of the method described by Wu and Hancock.<sup>50</sup> Briefly, overnight cultures of *S. aureus* DM4001 were grown to exponential phase and then harvested. Bacteria were suspended and washed with buffer solution (5 mM HEPES at pH 7) until an optical density of 0.09 at 622 nm ( $\text{OD}_{620}$ ) was obtained. The cell suspension was then incubated with 0.4  $\mu\text{M}$   $\text{DiSC}_3\text{-S}$  and 0.1 M potassium chloride (KCl) for 20 min at 37 °C with shaking. This compound has an excitation wavelength of 660 nm and an emission wavelength of 670 nm. Maximal uptake of  $\text{DiSC}_3\text{-S}$  was achieved when the reduction of fluorescence intensity became stable as a consequence of self-quenching in the untreated bacteria. The desired concentration of **3b** was then added into a stirred cuvette, and the change in fluorescence was monitored. DMF alone had no effect on depolarization. Experiments were repeated at least three times and found to be reproducible. Data from one experiment is presented.

**SYTOX Green Uptake Assay.** The protocol was based on the method of Rathinakumar et al.<sup>51</sup> Briefly, a clinical isolate of *S. aureus* was harvested at exponential phase. The bacteria were then suspended in 20 mM PBS until an optical density of 0.09 was obtained at 620 nm ( $\text{OD}_{620}$ ). The bacterial suspension was incubated with 3  $\mu\text{M}$  SYTOX Green (Invitrogen) in the dark. The mixture was then monitored in a stirring cuvette at an excitation wavelength of 504 nm and an emission wavelength of 523 nm. When the fluorescence signal was stabilized, 10  $\mu\text{M}$  of **2b** or **3b** was added, and the increase in SYTOX green fluorescence was measured. Experiments were repeated at least three times and found to be reproducible. Data from one experiment is presented.

**Visualization of Bacterial Permeabilization Using Fluorescence Microscopy.** The clinical isolate *S. aureus* DM4001 was suspended in PBS buffer (20 mM) until an  $\text{OD}_{620}$  of 0.4 was obtained. The suspension was then incubated with 10  $\mu\text{M}$  of **3b** or **2b** for 5 min. The treated bacteria were immobilized on poly(L-lysine)-coated glass slides, which were then examined using fluorescence microscopy (ZEISS model Axioplan 2 IE). An excitation wavelength of 485 nm was used.

**Molecular Dynamics (MD) Simulation.** To understand the interactions with the membrane at the molecular level, molecular dynamics simulations were carried out to study the interaction of **3b** with a model bacterial membrane. The model bacterial membrane was represented by 96 POPE and 32 POPG lipid molecules, as constructed by Zhao et al.<sup>55</sup> and used in our previous studies of  $\alpha$ -mangostin.<sup>10</sup> As in our previous studies concerning the membrane-targeting action of  $\alpha$ -mangostin, the bonded and LJ parameters of **3b** were generated using ATB<sup>71</sup> together with AM1 charges for the electrostatic interactions.<sup>72</sup> The lipid molecules were simulated using the Gromos63a6 force field, and water molecules were simulated using the SPC model.<sup>73</sup> Simulations were performed using 1 and 9 **3b** molecules, corresponding to low and high concentrations of **3b**, respectively. In both simulations, **3b** molecules with random orientations were positioned close to the model bacterial membrane. The system was then solvated with approximately 7000 water molecules and neutralized with sodium ions. The system was first subjected to 500 steps of energy minimization using the steep descent algorithm, followed by a 10 ps NVT simulation. Then, a 400 ns MD simulation was performed for both concentrations of **3b**. During the MD simulations, a cutoff distance of 1.2 nm was used for both the LJ and real-space electrostatic interactions, and the particle-mesh Ewald algorithm was used to calculate the long-range electrostatic interactions in reciprocal space. The Nose-Hoover method was used to maintain the target temperature at 310 K, and the Parrinello-Rahman method with semi-isotropic coupling was used to maintain the pressure at 1 atm in the NPT ensemble.

**In Vivo Toxicity Test Using Topical Application in Mice.** Wild-type C57BL6 (6–8 weeks old) mice were purchased from the National University of Singapore and used in this study. IACUC (SingHealth) approval was obtained for all animal studies, and procedures were conducted in compliance with the ARVO statement

for the Use of Animals in Ophthalmic and Vision Research and the Guide for the Care and Use of Laboratory Animals (National Research Council) under the supervision of the SingHealth Experimental Medical Center (SEMC). **3b** was dissolved in PBS to a concentration of 400  $\mu\text{g}/\text{mL}$ . Normal, healthy wild-type mice (6–8 weeks old) were used, and **3b** (400  $\mu\text{g}/\text{mL}$ ) was applied onto eyes topically 5 times over 1 day. At the end of the experiment, corneal clarity was examined by slit lamp microscopy.

**In Vivo Toxicity Test in a Rabbit Corneal Wound Healing Model.** New Zealand white rabbits (weighing 2–3 kg) were purchased from the National University of Singapore and used in this study. All animal studies were conducted in compliance with the ARVO statement for the Use of Animals in Ophthalmic and Vision Research and the Guide for the Care and Use of Laboratory Animals (National Research Council) under the supervision of the SingHealth Experimental Medical Centre (SEMC). Eight Rabbits were randomly divided into three groups: two rabbits treated with normal saline were used as a control group, three rabbits were treated with vancomycin (50  $\mu\text{g}/\text{mL}$ ), and three rabbits were treated with **3b** (50  $\mu\text{g}/\text{mL}$ ). The rabbits were tranquilized by intraperitoneal injection of 1 mL of ketamine (100 mg/mL) and 0.5 mL of xylazil (20 mg). Corneas were then anesthetized by topical administration of 1% xylocaine. A 5 mm trephine was used to outline the wound margin, and epithelial cells were mechanically removed using a sterile miniblade (BD-Beaver), leaving the basal lamina intact.<sup>74–77</sup> All three groups were treated by topical administration with their respective drugs 3 times per day. The time course of wound closure was determined from fluorescein staining photographs of the defect area. All photographs were taken at a fixed focal length using slit-lamp microscopy. All images were processed in Image-J version 1.44o, and outlines of the defect areas were plotted. The Mann-Whitney test was used to determine whether a difference in re-epithelialization existed between the three groups. The statistical calculations were performed using PASW statistic 18.

**In Vivo Acute Toxicity Test.** Wild-type C57BL6 (6–8 weeks old; 20–30 g) mice were purchased from the National University of Singapore and used in this study. All animals were placed in air-conditioned temperature-controlled rooms (23 ± 2 °C) with a 12 h light cycle and 55–60% humidity and acclimatized for 1 week before testing. All animal studies were conducted in compliance with the ARVO statement for the Use of Animals in Ophthalmic and Vision Research and the Guide for the Care and Use of Laboratory Animals (National Research Council) under the supervision of the SingHealth Experimental Medical Centre (SEMC). Normal, healthy wild type mice were chosen, and their weight was measured. A dose of 50 mg/kg of **3b** was dissolved in PBS and delivered by intraperitoneal injection. On the basis of the results of the intraperitoneal injections, **3b** (25 mg/kg) was chosen for intravenous administration. Two animals were used for each administration, and the animals were carefully monitored for 24 h to observe any mortality, morbidity, or toxicity. Gross necropsy was performed on any dead or moribund animal.<sup>78,79</sup>

## AUTHOR INFORMATION

### Corresponding Author

\*For R.W.B.: phone, (+65) 63224544; fax, (+65) 63224599; E-mail, [rwbeurman@gmail.com](mailto:rwbeurman@gmail.com). For S.L.: phone, (+65) 66012464; fax, (+65) 68723818; E-mail, [liushouping@gmail.com](mailto:liushouping@gmail.com). For D.C.: phone, (86) 20-8711-0245; fax, (86) 20-8711-0245; E-mail, [drcao@scut.edu.cn](mailto:drcao@scut.edu.cn).

### Present Addresses

<sup>†</sup>Department of Biological Sciences, National University of Singapore, 14 Science Drive 4, Singapore 117543, Singapore

<sup>‡</sup>School of Biological Sciences, Nanyang Technological University, 60 Nanyang Drive, Singapore 63755, Singapore

### Author Contributions

◆These authors contributed equally to this work.

### Notes

The authors declare no competing financial interest.

## ■ ACKNOWLEDGMENTS

This work was supported by NIG/NMRC grant R753, Exploit Flagship funding X031, NSFC (20872038, 21072064), and NMRC/TCR/002-SERI/2088R618. We thank Li Mei Pang for her assistance in performing the SYTOX Green assay and for helpful discussions. We also thank and Shuhaida Binte Mohamed Salleh for technical support in MIC determination and the time-kill study.

## ■ ABBREVIATIONS USED

MIC, minimum inhibitory concentration; MIC<sub>99</sub>, minimum inhibitory concentration required to inhibit the growth of 99% of organisms; CAMP, cationic antimicrobial peptide; MRSA, methicillin-resistant *Staphylococcus aureus*; VISA, vancomycin intermediate resistant *Staphylococcus aureus*; ATCC, American Type Culture Collection; LPS, lipopolysaccharide; cps, counts per second; MHB, Muller Hinton Broth; CFU, colony forming unit; OECD, The Organisation for Economic Co-operation and Development; ACN, acetonitrile

## ■ REFERENCES

- (1) Cosgrove, S. E.; Qi, Y.; Kaye, K. S.; Harbarth, S.; Karchmer, A. W.; Carmeli, Y. The impact of methicillin resistance in *Staphylococcus aureus* bacteremia on patient outcomes: mortality, length of stay, and hospital charges. *Infect. Control Hosp. Epidemiol.* **2005**, *26*, 166–174.
- (2) Xiao, Y. H.; Giske, C. G.; Wei, Z. Q.; Shen, P.; Heddini, A.; Li, L. J. Epidemiology and characteristics of antimicrobial resistance in China. *Drug. Resist. Update* **2011**, *14*, 236–250.
- (3) Levy, S. B.; Marshall, B. Antibacterial resistance worldwide: causes, challenges and responses. *Nature Med.* **2004**, *10*, S122–129.
- (4) Resch, A.; Wilke, M.; Fink, C. The cost of resistance: incremental cost of methicillin-resistant *Staphylococcus aureus* (MRSA) in German hospitals. *Eur. J. Health Econ.* **2009**, *10*, 287–297.
- (5) Hanberger, H.; Walther, S.; Leone, M.; Barie, P. S.; Rello, J.; Lipman, J.; Marshall, J. C.; Anzueto, A.; Sakr, Y.; Pickkers, P.; Engoren, M.; Vincent, J. L. Increased mortality associated with methicillin-resistant *Staphylococcus aureus* (MRSA) infection in the intensive care unit: results from the EPIC II study. *Int. J. Antimicrob. Agents* **2011**, *38*, 331–335.
- (6) Hidron, A. I.; Edwards, J. R.; Patel, J.; Horan, T. C.; Sievert, D. M.; Pollock, D. A.; Fridkin, S. K. NHSN annual update: antimicrobial-resistant pathogens associated with healthcare-associated infections: annual summary of data reported to the National Healthcare Safety Network at the Centers for Disease Control and Prevention, 2006–2007. *Infect. Control Hosp. Epidemiol.* **2008**, *29*, 996–1011.
- (7) Rozen, D. E.; McGee, L.; Levin, B. R.; Klugman, K. P. Fitness costs of fluoroquinolone resistance in *Streptococcus pneumoniae*. *Antimicrob. Agents Chemother.* **2007**, *51*, 412–416.
- (8) Meka, V. G.; Gold, H. S. Antimicrobial resistance to linezolid. *Clin. Infect. Dis.* **2004**, *39*, 1010–1015.
- (9) Hsu, L. Y.; Leong, M.; Balm, M.; Chan, D. S.; Huggan, P.; Tan, T. Y.; Koh, T. H.; Hon, P. Y.; Ng, M. M. Six cases of daptomycin-non-susceptible *Staphylococcus aureus* bacteraemia in Singapore. *J. Med. Microbiol.* **2010**, *59*, 1509–1513.
- (10) Koh, J.-J.; Qiu, S.; Zou, H.; Lakshminarayanan, R.; Li, J.; Zhou, X.; Tang, C.; Saraswathi, P.; Verma, C.; Tan, D. T. H.; Tan, A. L.; Liu, S.; Beuerman, R. W. Rapid bactericidal action of alpha-mangostin against MRSA as an outcome of membrane targeting. *Biochim. Biophys. Acta* **2013**, *1828*, 834–844.
- (11) Hurdle, J. G.; O'Neill, A. J.; Chopra, I.; Lee, R. E. Targeting bacterial membrane function: an underexploited mechanism for treating persistent infections. *Nature Rev. Microbiol.* **2011**, *9*, 62–75.
- (12) Eun, Y. J.; Foss, M. H.; Kiebusch, D.; Pauw, D. A.; Westler, W. M.; Thanbichler, M.; Weibel, D. B. DCAP: A Broad-Spectrum Antibiotic That Targets the Cytoplasmic Membrane of Bacteria. *J. Am. Chem. Soc.* **2012**, *134*, 11322–11325.
- (13) Bai, Y.; Liu, S.; Li, J.; Lakshminarayanan, R.; Pasmanabhan, S.; Tang, C.; Ho, D.; Verma, C.; Beuerman, R. W.; Pervushin, K. Progressive structuring of a branched antimicrobial peptide on the path to the inner membrane target. *J. Biol. Chem.* **2012**, *287*, 26606–26617.
- (14) Shai, Y. Mode of action of membrane active antimicrobial peptides. *Biopolymers* **2002**, *66*, 236–248.
- (15) Vooturi, S. K.; Firestone, S. M. Synthetic membrane-targeted antibiotics. *Curr. Med. Chem.* **2010**, *17*, 2292–300.
- (16) Wimley, W. C. Describing the mechanism of antimicrobial peptide action with the interfacial activity model. *ACS Chem. Biol.* **2010**, *5*, 905–917.
- (17) Epanand, R. M.; Vogel, H. J. Diversity of antimicrobial peptides and their mechanisms of action. *Biochim. Biophys. Acta* **1999**, *1462*, 11–28.
- (18) Brogden, K. A. Antimicrobial peptides: pore formers or metabolic inhibitors in bacteria? *Nature Rev. Microbiol.* **2005**, *3*, 238–250.
- (19) Hancock, R. E. W. Host Defence (Cationic) Peptides. What is Their Future Clinical Potential? *Drugs* **1999**, *57*, 469–473.
- (20) Ishitsuka, Y.; Arnt, L.; Majewski, J.; Frey, S.; Ratajczek, M.; Kjaer, K.; Tew, G. N.; Lee, K. Y. Amphiphilic poly-(phenyleneethynylene)s can mimic antimicrobial peptide membrane disordering effect by membrane insertion. *J. Am. Chem. Soc.* **2006**, *128*, 13123–13129.
- (21) Tew, G. N.; Clements, D.; Tang, H.; Arnt, L.; Scott, R. W. Antimicrobial activity of an abiotic host defense peptide mimic. *Biochim. Biophys. Acta* **2006**, *1758*, 1387–1392.
- (22) Ding, B.; Guan, Q.; Walsh, J. P.; Boswell, J. S.; Winter, T. W.; Winter, E. S.; Boyd, S. S.; Li, C.; Savage, P. B. Correlation of the antibacterial activities of cationic peptide antibiotics and cationic steroid antibiotics. *J. Med. Chem.* **2002**, *45*, 663–669.
- (23) Su, Y.; DeGrado, W. F.; Hong, M. Orientation, dynamics, and lipid interaction of an antimicrobial arylamide investigated by 19F and 31P solid-state NMR spectroscopy. *J. Am. Chem. Soc.* **2010**, *132*, 9197–205.
- (24) Hansen, T.; Alst, T.; Havelkova, M.; Strom, M. B. Antimicrobial activity of small beta-peptidomimetics based on the pharmacophore model of short cationic antimicrobial peptides. *J. Med. Chem.* **2010**, *53*, 595–606.
- (25) Isaksson, J.; Brandsdal, B. O.; Engqvist, M.; Flaten, G. E.; Svendsen, J. S.; Stensen, W. A synthetic antimicrobial peptidomimetic (LTX 109): stereochemical impact on membrane disruption. *J. Med. Chem.* **2011**, *54*, 5786–5795.
- (26) Schmidt, E. J.; Boswell, J. S.; Walsh, J. P.; Schellenberg, M. M.; Winter, T. W.; Li, C.; Allman, G. W.; Savage, P. B. Activities of cholic acid-derived antimicrobial agents against multidrug-resistant bacteria. *J. Antimicrob. Chemother.* **2001**, *47*, 671–674.
- (27) Hyz, K.; Kaweck, R.; Misior, A.; Bocian, W.; Bednarek, E.; Sitkowski, J.; Kozerski, L. Genistein binding mode to doubly nicked dumbbell DNA. Dynamic and diffusion ordered NMR study. *J. Med. Chem.* **2011**, *54*, 8386–8393.
- (28) Johnson, J. J.; Petiwala, S. M.; Syed, D. N.; Rasmussen, J. T.; Adhami, V. M.; Siddiqui, I. A.; Kohl, A. M.; Mukhtar, H. alpha-Mangostin, a xanthone from mangosteen fruit, promotes cell cycle arrest in prostate cancer and decreases xenograft tumor growth. *Carcinogenesis* **2012**, *33*, 413–419.
- (29) Jung, H. A.; Su, B. N.; Keller, W. J.; Mehta, R. G.; Kinghorn, A. D. Antioxidant xanthones from the pericarp of *Garcinia mangostana* (Mangosteen). *J. Agric. Food. Chem.* **2006**, *54*, 2077–2082.
- (30) Hall, H. K., Jr. Correlation of the Base Strengths of Amines. *J. Am. Chem. Soc.* **1957**, *79*, 5441–5444.
- (31) Salvatore, R. N.; Yoon, C. H.; Jung, K. W. Synthesis of secondary amines. *Tetrahedron* **2001**, *57*, 7785–7781.
- (32) Clayden, J.; Greeves, N.; Warren, S.; Wothers, P. *Organic Chemistry*; Oxford University Press: Oxford, UK, 2001; p 437.
- (33) Nikaido, H. Molecular basis of bacterial outer membrane permeability revisited. *Microbiol. Mol. Biol. Rev.* **2003**, *67*, 593–656.

- (34) Vaara, M. Agents that increase the permeability of the outer membrane. *Microbiol. Rev.* **1992**, *56*, 395–411.
- (35) Savage, P. B. Multidrug-resistant bacteria: overcoming antibiotic permeability barriers of Gram-negative bacteria. *Ann. Med.* **2001**, *33*, 167–171.
- (36) Djouhri-Bouktab, L.; Vidal, N.; Rolain, J. M.; Brunel, J. M. Synthesis of New 3,20-Bispolymyaminosteroid Squalamine Analogues and Evaluation of Their Antimicrobial Activities. *J. Med. Chem.* **2011**, *54*, 7417–7421.
- (37) Schofield, K.; Grimmett, M. R.; Keene, B. R. T. *Heteroaromatic Nitrogen Compounds: The Azoles*; Cambridge University Press: London, 1976; pp 281–284.
- (38) Dharmaratne, H. R.; Sakagami, Y.; Piyasena, K. G.; Thevanesam, V. Antibacterial activity of xanthenes from *Garcinia mangostana* (L.) and their structure–activity relationship studies. *Nat. Prod. Res.* **2012**, *1*–4.
- (39) Vooturi, S. K.; Cheung, C. M.; Rybak, M. J.; Firestone, S. M. Design, synthesis, and structure–activity relationships of benzophenone-based tetraamides as novel antibacterial agents. *J. Med. Chem.* **2009**, *52*, 5020–5031.
- (40) *Partition Coefficient (n-Octanol/Water), HPLC Method*, Organisation for Economic Co-operation and Development, Test No. 117; OECD Publishing: Paris, 2004; p 11.
- (41) Liu, S.; Zhou, L.; Chen, L.; Dastidar, S. G.; Verma, C.; Li, J.; Tan, D.; Beuerman, R. Effect of structural parameters of peptides on dimer formation and highly oxidized side products in the oxidation of thiols of linear analogues of human beta-defensin 3 by DMSO. *J. Pept. Sci.* **2009**, *15*, 95–106.
- (42) Zhou, L.; Liu, S. P.; Chen, L. Y.; Li, J.; Ong, L. B.; Guo, L.; Wohland, T.; Tang, C. C.; Lakshminarayanan, R.; Mavinahalli, J.; Verma, C.; Beuerman, R. W. The structural parameters for antimicrobial activity, human epithelial cell cytotoxicity and killing mechanism of synthetic monomer and dimer analogues derived from hBD3 C-terminal region. *Amino Acids* **2011**, *40*, 123–133.
- (43) Hiramatsu, K.; Hanaki, H.; Ino, T.; Yabuta, K.; Oguri, T.; Tenover, F. C. Methicillin-resistant *Staphylococcus aureus* clinical strain with reduced vancomycin susceptibility. *J. Antimicrob. Chemother.* **1997**, *40*, 135–136.
- (44) Grohs, P.; Kitzis, M. D.; Gutmann, L. In vitro bactericidal activities of linezolid in combination with vancomycin, gentamicin, ciprofloxacin, fusidic acid, and rifampin against *Staphylococcus aureus*. *Antimicrob. Agents Chemother.* **2003**, *47*, 418–420.
- (45) Chin, J. N.; Rybak, M. J.; Cheung, C. M.; Savage, P. B. Antimicrobial activities of ceragenins against clinical isolates of resistant *Staphylococcus aureus*. *Antimicrob. Agents Chemother.* **2007**, *51*, 1268–1273.
- (46) Clardy, J.; Fischbach, M. A.; Walsh, C. T. New antibiotics from bacterial natural products. *Nature Biotechnol.* **2006**, *24*, 1541–1550.
- (47) Zasloff, M. Antimicrobial peptides of multicellular organisms. *Nature* **2002**, *415*, 389–395.
- (48) Farrell, D. J.; Robbins, M.; Rhys-Williams, W.; Love, W. G. Investigation of the potential for mutational resistance to XF-73, retapamulin, mupirocin, fusidic acid, daptomycin, and vancomycin in methicillin-resistant *Staphylococcus aureus* isolates during a 55-passage study. *Antimicrob. Agents Chemother.* **2011**, *55*, 1177–1181.
- (49) von Nussbaum, F.; Brands, M.; Hinzen, B.; Weigand, S.; Habich, D. Antibacterial natural products in medicinal chemistry—exodus or revival? *Angew. Chem., Int. Ed. Engl.* **2006**, *45*, 5072–5129.
- (50) Wu, M.; Hancock, R. E. Interaction of the cyclic antimicrobial cationic peptide bactenecin with the outer and cytoplasmic membrane. *J. Biol. Chem.* **1999**, *274*, 29–35.
- (51) Rathinakumar, R.; Walkenhorst, W. F.; Wimley, W. C. Broad-spectrum antimicrobial peptides by rational combinatorial design and high-throughput screening: the importance of interfacial activity. *J. Am. Chem. Soc.* **2009**, *131*, 7609–7617.
- (52) Roth, B. L.; Poot, M.; Yue, S. T.; Millard, P. J. Bacterial viability and antibiotic susceptibility testing with SYTOX green nucleic acid stain. *Appl. Environ. Microbiol.* **1997**, *63*, 2421–2431.
- (53) Yenugu, S.; Hamil, K. G.; Radhakrishnan, Y.; French, F. S.; Hall, S. H. The androgen-regulated epididymal sperm-binding protein, human beta-defensin 118 (DEFB118) (formerly ESC42), is an antimicrobial beta-defensin. *Endocrinology* **2004**, *145*, 3165–3173.
- (54) Cotroneo, N.; Harris, R.; Perlmutter, N.; Beveridge, T.; Silverman, J. A. Daptomycin exerts bactericidal activity without lysis of *Staphylococcus aureus*. *Antimicrob. Agents Chemother.* **2008**, *52*, 2223–2225.
- (55) Zhao, W.; Rog, T.; Gurtovenko, A. A.; Vattulainen, I.; Karttunen, M. Role of phosphatidylglycerols in the stability of bacterial membranes. *Biochimie* **2008**, *90*, 930–938.
- (56) Som, A.; Tew, G. N. Influence of lipid composition on membrane activity of antimicrobial phenylene ethynylene oligomers. *J. Phys. Chem. B* **2008**, *112*, 3495–3502.
- (57) Penha, F. M.; Rodrigues, E. B.; Maia, M.; Furlani, B. A.; Regatieri, C.; Melo, G. B.; Magalhaes, O., Jr.; Manzano, R.; Farah, M. E. Retinal and ocular toxicity in ocular application of drugs and chemicals—part II: retinal toxicity of current and new drugs. *Ophthalmic Res.* **2010**, *44*, 205–224.
- (58) Etter, J. C.; Gloor, S.; Mayer, J. M. The adverse effects of local anesthetics on the eye in the development of ocular irritation test. *Pharm. Acta Helv.* **1992**, *67*, 242–249.
- (59) Etter, J. C.; Wildhaber, A. Biopharmaceutical test of ocular irritation in the mouse. *Food. Chem. Toxicol.* **1985**, *23*, 321–323.
- (60) Furrer, P.; Plazonnet, B.; Mayer, J. M.; Gurny, R. Application of in vivo confocal microscopy to the objective evaluation of ocular irritation induced by surfactants. *Int. J. Pharm.* **2000**, *207*, 89–98.
- (61) Alfonso, E. C.; Albert, D. M.; Kenyon, K. R.; Robinson, N. L.; Hanninen, L.; D'Amico, D. J. In vitro toxicity of gentamicin to corneal epithelial cells. *Cornea* **1990**, *9*, 55–61.
- (62) Nakamura, M.; Nishida, T.; Mishima, H.; Otori, T. Effects of antimicrobials on corneal epithelial migration. *Curr. Eye Res.* **1993**, *12*, 733–740.
- (63) Petroustos, G.; Guimaraes, R.; Giraud, J.; Pouliquen, Y. Antibiotics and corneal epithelial wound healing. *Arch. Ophthalmol.* **1983**, *101*, 1775–1778.
- (64) Mallari, P. L.; McCarty, D. J.; Daniell, M.; Taylor, H. Increased incidence of corneal perforation after topical fluoroquinolone treatment for microbial keratitis. *Am. J. Ophthalmol.* **2001**, *131*, 131–133.
- (65) Konishi, M.; Yamada, M.; Mashima, Y. Corneal ulcer associated with deposits of norfloxacin. *Am. J. Ophthalmol.* **1998**, *125*, 258–260.
- (66) Eiferman, R. A.; Snyder, J. P.; Nordquist, R. E. Ciprofloxacin microprecipitates and macroprecipitates in the human corneal epithelium. *J. Cataract Refract. Surg.* **2001**, *27*, 1701–1702.
- (67) Pini, A.; Giuliani, A.; Falciani, C.; Fabbri, M.; Pileri, S.; Lelli, B.; Bracci, L. Characterization of the branched antimicrobial peptide M6 by analyzing its mechanism of action and in vivo toxicity. *J. Pept. Sci.* **2007**, *13*, 393–399.
- (68) Zanetti, M.; Gennaro, R.; Skerlavaj, B.; Tomasinsig, L.; Circo, R. Cathelicidin Peptides as Candidates for a Novel Class of Antimicrobials. *Curr. Pharm. Des.* **2002**, *8*, 779–793.
- (69) Morino, T.; Sano, K.; Hara, H.; Motoyama, K.; Lizuka, K.; Hara, T.; Matsumoto, K.; Yamamoto, H. Toxicological studies on isepamicin (HAPA-B). I. Acute toxicity test in the mouse, rat and dog. *Jpn. J. Antibiot.* **1986**, *12*, 3164–3178.
- (70) Liu, S. P.; Zhou, L.; Li, J.; Suresh, A.; Verma, C.; Foo, Y. H.; Yap, E. P. H.; Tan, D. T. H.; Beuerman, R. W. Linear analogues of human beta-defensin 3: concepts for design of antimicrobial peptides with reduced cytotoxicity to mammalian cells. *ChemBioChem* **2008**, *9*, 964–973.
- (71) Malde, A. K.; Zuo, L.; Breeze, M.; Stroet, M.; Poger, D.; Nair, P. C.; Oostenbrink, C.; Mark, A. E. An Automated Force Field Topology Builder (ATB) and Repository: Version 1.0. *J. Chem. Theory Comput.* **2011**, *7*, 4026–4037.
- (72) Lemkul, J. A.; Allen, W. J.; Bevan, D. R. Practical considerations for building GROMOS-compatible small-molecule topologies. *J. Chem. Inf. Model.* **2010**, *50*, 2221–2235.



(73) Berendsen, H.; Postma, J.; Gunsteren, W. v.; Hermans, J. In *Intermolecular Forces*; Pullman, B., Ed.; Reidel: Dordrecht, The Netherlands, 1981.

(74) Frantz, J. M.; Dupuy, B. M.; Kaufman, H. E.; Beuerman, R. W. The effect of collagen shields on epithelial wound healing in rabbits. *Am. J. Ophthalmol.* **1989**, *108*, 524–528.

(75) Brazzell, R. K.; Stern, M. E.; Aquavella, J. V.; Beuerman, R. W.; Baird, L. Human recombinant epidermal growth factor in experimental corneal wound healing. *Invest. Ophthalmol. Vis. Sci.* **1991**, *32*, 336–340.

(76) Crosson, C. E.; Klyce, S. D.; Beuerman, R. W. Epithelial wound closure in the rabbit cornea. A biphasic process. *Invest. Ophthalmol. Vis. Sci.* **1986**, *27*, 464–473.

(77) Reidy, J. J.; Zarzour, J.; Thompson, H. W.; Beuerman, R. W. Effect of topical beta blockers on corneal epithelial wound healing in the rabbit. *Br. J. Ophthalmol.* **1994**, *78*, 377–380.

(78) Gad, S. C.; Chengelis, C. P. *Acute Toxicology Testing*, 2nd ed.; Elsevier Inc.: New York, 1998; pp 221–256.

(79) Kratz, F.; Ehling, G.; Kauffmann, H. M.; Unger, C. Acute and repeat-dose toxicity studies of the (6-maleimidocaproyl)hydrazone derivative of doxorubicin (DOXO-EMCH), an albumin-binding prodrug of the anticancer agent doxorubicin. *Hum. Exp. Toxicol.* **2007**, *26*, 19–35.